The analysis of Last Interglacial (MIS 5e) relative sea-level indicators: reconstructing sea-level in a warmer world

Alessio Rovere[1,2,3], Maureen E. Raymo[3], Matteo Vacchi[4], Thomas Lorscheid[1,2], Paolo Stocchi[5], Lluís Gómez-Pujol [6], Daniel L. Harris[1,2], Elisa Casella[2], Michael J. O'Leary[7], Paul J. Hearty[8].

Affiliations

1 MARUM, University of Bremen, Leobener Straße, 28359, Bremen, Germany.

2 ZMT, Leibniz Center for Tropical Marine Ecology, Fahrenheitstraße 6, 28359 Bremen, Germany

3 Lamont-Doherty Earth Observatory, Columbia University, 61 Route 9W, Palisades, NY 10964, United States

4 Aix-Marseille Université, CEREGE CNRS-IRD UMR 34, Europole de l'Arbois BP 80, 13545 Aix-en-Provence, Cedex 4, France.

5 NIOZ, NIOZ Royal Netherlands Institute for Sea Research, 1790AB Den Burg, Texel, Netherlands

6 SOCIB, Balearic Islands Coastal Observing and Forecasting System. ParcBit, Ed. Naorte, Ctra. Valldemossa km 7.4, 07121 Palma (Balearic Islands), Spain.

7 Department of Environment and Agriculture, Curtin University, Perth, Australia

8 Environmental Studies department at the University of North Carolina, Wilmington, United States

Keywords: Last Interglacial; paleo sea-level; Sea-level marker; MIS 5e; Sea-level reconstruction; Ice sheets; past sea-level changes

Abstract

The Last Interglacial (MIS 5e, 128-116 ka) is among the most studied past periods in Earth's history. The climate at that time was warmer than today, primarily due to different orbital conditions, with smaller ice sheets and higher sea-level. Field evidence for MIS 5e sea-level was reported from thousands of sites, but often paleo shorelines were measured with low-accuracy techniques and, in some cases, there are contrasting interpretations about paleo sea-level reconstructions. For this reason, large uncertainties still surround both the maximum sea-level attained as well as the pattern of sea-level change throughout MIS 5e. Such uncertainties are exacerbated by the lack of a uniform approach to measuring and interpreting the geological evidence of paleo sea-levels. In this review, we discuss the characteristicsof MIS 5e field observations, and we set the basis for a standardized approach to MIS 5e paleo sea-level reconstructions, that is already successfully applied in Holocene sea-level research. Application of the standard definitions and methodologies described in this paper will enhance our ability to compare data from different research groups and different areas, in order to gain deeper insights into MIS 5e sea-level changes. Improving estimates of Last Interglacial sea-level is, in turn, a key to understand the behavior of ice sheets in a warmer world.

1. Introduction

Past interglacials are of interest to the scientific community as they can be used to study the behavior of the climate system during times as warm as or slightly warmer than today. Of particular interest is the degree to which relatively small perturbations to climate forcing variables such as atmospheric or sea surface temperature, insolation, or CO_2 can lead to polar ice volume and sea-level changes. For instance, during marine isotope stage (MIS) 5e, the Last Interglacial (LIG, ~128 to 116 ka , Stirling et al., 1998), ice core evidence suggests greenhouse gas concentrations were slightly higher than pre-industrial levels (Petit et al., 1999) and summer insolation at high latitudes was also higher by ~10%. These small changes in climate forcing were apparently sufficient to warm polar temperatures (>66° latitude) in both hemispheres by about 3-5 °C relative to today (Otto-Bliesner et al., 2006) and global mean temperature by an estimated 1.5°C (Turney and Jones, 2010, Lunt et al., 2013). By comparison, global mean temperature has increased by about half this, or by ~0.85°C, since 1880 (IPCC, 2013) and an additional global warming of 1°C, that could be expected to raise polar temperatures by 3-6 °C (Kattsov et al., 2005), is likely to occur by the end of this century. Indeed, the Antarctic Peninsula has been warming by an average of 0.5°C per decade over the last 60 years (Mulvaney et al., 2013).

There is increasing evidence suggesting that the MIS 5e climatic conditions resulted in smaller ice sheets and, therefore, higher than present sea-levels (e.g., Kopp et al., 2009). The study of sea-level indicators dating from the Last Interglacial, therefore, is fundamental to unravel potential patterns of future sea-level rise caused by global warming (IPCC 2013). The only direct observations that allow reconstruction of MIS 5e sea-levels are features associated with paleo sea-levels such as, for example, fossil coral reef terraces (Murray-Wallace and Woodroffe, 2014). However, reconstructing MIS 5e sea-level from such observations carries uncertainties related to age attribution and to how sea-level indicators are measured and interpreted by field geologists.

Two main issues are related to the methods used to establish the elevation of a sea-level indicator, as well as how precisely those measurements are referred to modern mean sea-level. Standard topographic techniques (e.g. differential GPS, with vertical accuracy down to a few centimeters) have been employed

in Pleistocene and Pliocene field studies only recently and therefore measurement errors reported by older studies need to be re-assessed. A fundamental issue relates to how paleo sea-level is calculated from the elevation of an indicator. Indeed, most MIS 5e (and older) markers cannot be correlated precisely to a tidal datum as happens, for example, with particular foraminifera assemblages in Holocene salt marshes (Shennan and Horton, 2002) or with coral microatolls (Woodroffe et al., 2012; Mann et al., 2016). Most MIS 5e sea-level indicators carry with them large sea-level uncertainties that are often not reported or properly defined.

The overall aim of this paper is to give a complete account of the best field practices that should be adopted when surveying MIS 5e and older sea-level indicators. In this study we aim to:

- **i) Present a set of definitions and standardizations** that should be adopted in MIS 5e sea-level studies. Adopting such definitions both in studies reporting new sea-level indicators as well as in literature reviews will ensure that the results will be easily integrated in sea-level databases (Düsterhus et al., 2016).
- **ii) Describe the most common landforms and deposits** used as MIS 5e sea-level indicators, together with their upper and lower limits of formation under modern conditions.
- **iii) Present an example** of how the standard methodology described in this paper can be applied to a real study case.
- **iv) Discuss** the implications for paleoclimate reconstructions of adopting correct procedures in the measurement and reporting of MIS 5e datasets.

2. Definitions

Today, processes acting near modern mean sea-level (MSL) are shaping a set of landforms on both rocky and sedimentary coasts. These features include, for example, shore platforms or cobble beaches. When these features are found in the geologic record, disconnected from their environment of formation (for instance, a shore platform observed several meters above present-day sea-level), we infer that a **Relative Sea-Level (RSL)** change has occurred. Any elevation difference between the original and the present-day elevation of similar features is called **RSL change**. RSL changes may be caused by factors such as ice volume changes, isostatic crustal adjustments, tectonics or compaction-related subsidence. Any stratigraphic horizon, landform, or paleobiologic indicator of past sea-level is called an **RSL indicator** (or RSL marker). An RSL indicator must have at least three properties:

- i) its elevation needs to be referred to a known height datum, and its position (latitude and longitude) needs to be referred to a known geographic system;
- ii) its offset (relative or absolute) from a former sea-level needs to be known;
- iii) the age (relative or absolute) of the RSL indicator needs to be established with radiometric methods (such as ^{230}Th/U dating) or through chronostratigraphic correlation with other dated features.

Note that a RSL indicator is a more general form of 'sea-level index point', a concept used in Holocene sea-level studies (Shennan and Horton, 2002; Engelhart et al., 2009; Hijma et al., 2015). If the first two properties listed above are known, it is possible to calculate the paleo RSL (and its uncertainties) from the elevation of the RSL indicator (Table 1, Eqs. 1-4). This paleo RSL is still uncorrected for post-depositional land movements (PD) or glacial isostatic adjustment effects (GIA). To correct for these

processes, or obtain one of them from the RSL record, one must also know the age of the RSL indicator (see section 4) and apply a workflow that includes the Eqs. 5-8 (see applied example in Section 5). Post-depositional land movements include all the vertical displacements that have happened since the RSL indicator was deposited or shaped. These may include local or regional tectonic effects, sediment compaction, isostatic response to sediment loading or unloading (Dalca et al., 2013) and dynamic topography (Moucha et al., 2008; Rovere et al., 2015b; Rowley et al., 2013).

Any geological study on MIS 5e shorelines should aim to obtain the most accurate estimate of paleo RSL and its associated uncertainties. In the next section we describe how this can be achieved using field procedures and a standardized approach to the calculation of uncertainties.

2.1 Measuring the elevation of last interglacial RSL indicators

The elevation of an RSL indicator is the vertical distance between the marker and modern mean sea-level, while the elevation error represents the accuracy of the measurement itself. Every measurement needs to be referred to a vertical datum (i.e. a 'zero' reference frame, representing modern MSL). In literature, the survey instruments used to establish elevation, their accuracy, and the vertical datum used are seldom reported.

Several instruments can be used to measure the elevation of a RSL indicator—they vary in accuracy and in the ease with which they can be precisely related to a vertical datum (Table 2). The best measurement technique is represented by differential global positioning systems (DGPS) that can determine elevations either in real time or via post-processing (Muhs et al., 2014, 2011; O'Leary et al., 2013; Rovere et al., 2014b; Rovere et al., 2015b). DGPS elevation measurements can be referred to either a global geoid model (currently, EGM2008, Pavlis et al., 2012) or, where available, a local geoid model typically calculated by national geodetic institutes (http://www.isgeoid.polimi.it/). If a local geoid model is not available, one should calibrate the GPS measurements against a known tidal datum using the procedure described in Foster, 2015 (Handbook of Sea-level Research, Chapter 10.4.2, page 166-167, Figure 10.1). Errors in elevation measurements with DGPS typically range between 0.02 and 0.08 m depending on the differential positioning technique used as well as other factors such as the spatial distribution of satellites at the time of measurement or the presence of obstacles masking the satellite view (e.g. trees, buildings).

Other common survey instruments used to measure paleo shorelines (Table 2) are Total stations (Dutton et al., 2015), metered tapes or rods (Antonioli et al., 2006, their Fig. 5b), hand or auto levels (often combined with other more precise techniques such as DGPS, Dutton et al., 2015; O'Leary et al., 2008), and barometric altimeters (Pedoja et al., 2011b). With each of these methods, an estimate of the vertical error can be obtained through replication the measurement, followed by calculation of the mean and standard deviation of the measured elevations. This practice is not often followed. Furthermore, these techniques do not provide elevations that are directly referenced to a global or local geoid, but rather provide a measurement relative to a local starting point—a point that must then be benchmarked against a tidal datum (see Dutton et al., 2015 for an example).

To measure the elevation of large-scale landforms (such as marine terraces extending hundreds of meters to kilometers) one can employ topographic maps and Digital Elevation Models (DEMs).

Depending on the scale of the map or the grid size of the DEM, errors can range up to several meters. However, these techniques are particularly useful in tracking landforms at landscape scale, in order to identify possible warping or differential uplift due to tectonics or other post-depositional movements (Muhs et al., 1992; Rovere et al., 2015b). Airborne LIDAR datasets can be used for a similar purpose, with the advantage of a higher vertical accuracy (± a few centimeters, dependent on the specific laser sensor employed, GPS positioning and Inertial Measurement Unit). Recent developments in DEMs obtained from satellite imagery are providing elevations with a vertical accuracy < 1.5m and 1m grid spacing (e.g., DEMs derived from tri-stereo *Pleiades* satellite imagery).

2.2 Determining indicative meaning of a sea-level indicator according to the modern analog

After accurate elevation measurements of paleo RSL features are made, one must then evaluate where, relative to sea-level, those features formed (e.g., was the feature forming exactly at sea-level, above, or below it?). While the elevation measurement (and associated error) of any RSL indicator is an objective measure, the estimation of paleo RSL from a RSL indicator can be more subjective, commonly reported in sea-level studies as the 'geologic interpretation' of the data and thus more likely to give rise to controversy.

It is then important to introduce here the concept of indicative meaning. This is the most fundamental elevation attribute in RSL reconstructions and describes where, with respect to tide levels, the sea-level indicator formed (Shennan, 1982; Van de Plassche, 1986; Hijma et al., 2015). The indicative meaning consists of two parameters: the indicative range (IR) and reference water level (RWL). IR and RWL are concepts that are already widely applied in Holocene sea-level studies (Shennan and Horton, 2002; Engelhart and Horton, 2012; Vacchi et al., 2016) and are beginning to be employed in sea-level studies focused on older periods (Kopp et al., 2009; Rovere et al., 2015b). These terms can be defined as follows (Hijma et al., 2015):

The **IR** is the elevation range over which an indicator forms and the **RWL** is the mid- point of this range, expressed relative to the same datum as the elevation of the sampled indicator (geodetic datum or tide level). The greater the indicative range, the greater the uncertainty in the final paleo RSL reconstruction.

The **indicative meaning** for a given type of feature is determined by measuring its relationship with a specific contemporary tidal level (usually the mean sea-level, MSL) along the modern shorelines (i.e. the modern analog). The application of the concept of modern analog to Holocene sea-level studies has allowed the development of transfer function techniques, which have significantly improved our ability to assess, in a quantitative and standardized way, Holocene RSL changes (Juggins and Birks, 2012; Kemp and Talfords, 2015).

As an example, we assume in Figure 1 that a last interglacial exposed beach deposit (yellow unit in Figure 1) contains corals that were sampled and dated (e.g. with ^{230}Th/U) to MIS 5e. The beach deposit is found in close proximity to the inner margin of a marine terrace (red dot), which is used as RSL indicator. The measured elevation of the inner margin is +2.12±0.13 m. In the modern shoreline adjacent to the paleo RSL indicator, the inner margin of a terrace mantled by a shallow submerged beach deposit is defined as the modern analog. We observe that the modern inner margin is located between -0.9 and -1.8 m below

MSL depending upon where along the coast we are. In the lower left corner of Figure 1 we show how we can use the upper and lower limits for the RSL indicator to calculate RWL and IR using Eq.1 and Eq.2 (Table 1). Once IR and RWL are determined, it is possible to calculate the Paleo RSL index point and its associated uncertainty using Eqs.3 and 4 in Table 1 (i.e., an index point is a point that estimates relative sea-level at a specified time and place, cf. Gehrels and Long, 2007; Hijma et al., 2015).

In this example, we calculate the paleo RSL index point, and associated error, using Eq. 1-4 in Table 1, resulting in a paleo RSL elevation of +3.5±0.5 m (e.g. 2.12 m - (-1.35) = 3.5). It is worth noting that the final paleo RSL is 1.35 m higher than the initial measurement of marker elevation, obviously taking into account that the inner margin of a marine terrace forms on average at -1.35 meters in the modern local setting. In terms of ice sheet melting, this difference is significant, equal to roughly half of the proposed Greenland contribution to MIS 5e sea-level (Rybak and Huybrechts, 2013). A second aspect worth highlighting regards the number of significant digits with which we can approximate paleo RSL. While in the measured elevation, IR and RWL can be indicated with centimetric precision (i.e. 2.12m) if derived from high-accuracy instruments (e.g. DGPS), we suggest that the calculated paleo RSL should be indicated with decimetric precision, as it is unlikely that the calculations from Eqs. 1-4 can yield, for MIS 5e, values that are accurate at centimeter level.

Application of the indicative meaning approach to the interpretation of past sea-level requires the assumption that the local conditions responsible for the shaping of the landform, such as tidal or wave regime, have not changed significantly between the two times. It is possible that in some cases this assumption is not true, for example if higher sea-level during the Last Interglacial resulted in major changes in the paleogeography of the study area and therefore changes in how wave action or different tidal ranges may have influenced the formation of a marker. In this case, corrective factors with respect to the modern analog would need to be adopted (and of course described).

In order to calculate both IR and RWL, it is necessary to couple site-specific research on paleo sea-levels with that on modern shoreline processes, existing landforms and/or biological zonation of living organisms. Such information can be obtained by performing surveys on the modern shoreline, identifying, if present, the same facies and organisms encountered in the paleo record and measuring their modern elevation range. This approach was used, for example, by O'Leary et al., 2013, who measured the elevation (relative to MSL) of modern biological communities and geomorphic features in Western Australia, and then used these observed offsets to estimate the position of paleo RSL as indicated by the same facies in the fossil record (see Fig. 2 of O'Leary et al., 2013 for details).

Another site-specific approach involves the use of data available in literature to establish the boundaries of specific landforms. As an example, Rovere et al., 2015b inferred the indicative meaning for the mid-Pliocene shoreline scarp on the US Atlantic Coastal Plain referring to studies of modern beach profile variations at different places along the modern shoreline in the same region. On the modern shoreface, a major break in slope is observed at 3–7 m depth (Hallermeier, 1981; Larson and Kraus, 1994; Lee et al., 1998) that corresponds to the maximum water depth for nearshore erosion caused by average wave conditions. Using -3 and -7 meters as upper and lower limits of the IR, they calculated paleo RSL and associated uncertainties using Eqs. 1-4 in Table 1.

It is worth noting that paleo RSL indicators exclude those landforms that cannot be directly related to sea-level. As an example, a dune deposit will always be located above sea-level, but it is not possible to quantify with any useful accuracy where the dune was forming relative to the MSL. Such indicators are defined as **terrestrial limiting points**. Similarly, a marine deposit with *in situ* fauna with no stratigraphic or sedimentologic information that would allow one to tie it closely to sea-level must be considered as a **marine limiting point**. The only information that can be derived from terrestrial and marine limiting points is that, at the time of their formation, sea-level was respectively above or below the elevation of such indicators (Figure 2).

3. Last Interglacial RSL indicators

Scientific observations of late Quaternary, and particularly MIS 5e, shorelines higher than present date back almost two centuries (Darwin, 1846; Hutton, 1885; Lyell, 1837). Since then, numerous papers have addressed Last Interglacial relative sea-levels. Pedoja et al., 2014 compiled the most extensive review of paleo sea-level studies to date, identifying 987 studies that reported at least the elevation of an MIS 5e site. It is worth noting that the number of such studies increased dramatically in the decade 1970-1980, and has been growing steadily since (Figure 3c). Analyzing the Pedoja et al., 2014 database in a spatial context, we can identify the areas where the most MIS 5e sites are concentrated (Figure 3a). These include the west coast of the US (Muhs et al., 2004), the western Mediterranean Sea (Ferranti et al., 2006; Zazo et al., 2003) and the Japanese coasts (Ota and Omura, 1991). Relevant compilations of shoreline data at a regional scale include Ferranti et al., 2006; Hearty et al., 2007; Muhs et al., 2004; Murray-Wallace and Belperio, 1991; O'Leary et al., 2013, while more recent reviews are centered mostly on the timing of MIS 5e sea-level changes (e.g., Dutton and Lambeck, 2012; Medina-Elizalde, 2013; Hibbert et al., 2014).

Several problems are encountered when comparing MIS 5e data from different compilations. The main issue is that each MIS 5e database uses a different table structure as well as varying definitions of landforms and of their indicative meaning. Often, no distinction is given between measurement of the RSL indicator and the interpretation (e.g. the IR and RWL), although some observations that might inform the determination of indicative meaning are sometimes included in the description of the landforms (e.g. see Supplementary Data in Pedoja et al., 2014, 2011a, or main paper in Ferranti et al., 2006). In addition, the measurement methods adopted by authors and the vertical datum to which they reference their field elevation measurements are seldom described in detail, thus it is very difficult to assess measurement error in published studies.

Very few studies published prior to 2010 used high-precision techniques (e.g. differential GPS) to measure the elevation of RSL indicators or reported uncertainties associated with elevation measurements. Pedoja et al., 2014 (their Suppl. Data) highlight that, in their sea-level database, they '*systematically attributed a minimum error range of one meter to the measurements on elevation published without any margin of error*'. Among the sites they reviewed, almost half (456 over 943) have error bars equal to ±0.5 m (Figure 3d). In another large MIS 5e database, Kopp et al., 2009 included only sites where published information was detailed enough to derive a measurement error, IR and RWL. As a result, the number of sites in their database is much lower than in Pedoja's (78 data points vs 943), however, they presumably are much more accurate.

Major research need is to re-evaluate the measurement error of published data and perform new topographic measurements (e.g. with differential GPS, or a total station benchmarked to tidal gauges) in order to minimize the uncertainties in paleo sea leve estimates related to measurement error. Differential GPS instruments are becoming more accessible both in terms of usability by non-experts as well as cost (Stempfhuber and Buchholz, 2012; Takasu and Yasuda, 2009).

A common denominator of MIS 5e studies and databases is the relatively low number of landforms and deposits that have been used as RSL indicators (Figure 4, Table 3). For each one of these indicators, it is possible, in theory, to define their IRs relative to modern sea-level by studying modern analogs. This information can then be used to calculate paleo RSL with more rigorously determined uncertainties. In the next sections, we describe the most common RSL indicators that have been used in MIS 5e studies and we address, for each one, how upper and lower bounds of their indicative range can be calculated or estimated.

3.1 Marine terraces

Any relatively flat surface of marine origin can be defined a marine terrace (Pirazzoli, 2005, Figure 4a). Marine terraces can be shaped by marine erosion (wave-cut terraces) or can consist of shallow water to slightly emerged accumulations of materials redistributed by shore erosional and depositional processes (i.e., marine-built terraces) (Pirazzoli, 2005). Marine terraces range in width from few hundreds of meters to up to 1-2 kilometers, are often mantled by subtidal, intertidal or slightly supratidal deposits, and can stretch along many kilometers of coastline. They are widely used in sea-level studies, especially those addressing coastal uplift (Gaki-Papanastassiou et al., 2009; Kern, 1977; Ku and Kern, 1974; Muhs and Szabo, 1982; Muhs et al., 1992; Schellmann and Radtke, 2000; Zazo et al., 2007, 1999).

The feature of a marine terrace that is most commonly used as the paleo RSL indicator is the inner margin (Figure 5a), specifically the knickpoint between the sub-horizontal surface of the terrace and the vertical or sub-vertical landward cliff. If a relict inner margin is covered by colluvium deposits after its formation, the precision of the sea-level reconstruction necessarily decreases (see the example of the reconstruction of mid-Pliocene sea-level from the inner margin of the Orangeburg scarp, a Pliocene marine surface on the Atlantic Coastal Plain of the US, Rovere et al., 2015). In such cases, the thickness of the colluvium can be estimated independently, or it can be surveyed with indirect techniques such as ground penetrating radar (e.g. O'Neal and Dunn, 2003).

Along modern shorelines, it is possible to observe the inner margin of marine terraces in two settings. The first is above sea-level, usually bounded by a beach (Figure 5b). The inner margin can also be found below sea-level in the zone where marine abrasion is still active (Figure 5c; Ferranti et al 2006). Therefore, the upper limit of the indicative range for the inner margin of a marine terrace can be set to the storm wave swash height (SWSH), while the lower limit can be set to the breaking depth of significant waves that form the terrace (d_b, i.e. the depth at which waves start breaking; Smith, 2003; Vacchi et al., 2014). The sea-level information may be more precise if other features, such as *in situ* biological indicators, are found in proximity to the inner margin or knickpoint.

3.2 Coral reef terraces

Coral reef terraces can be considered a particular type of marine terrace (Figure 4b) as they are formed by the interplay of erosive processes (wave abrasion, bioerosion) and bioconstructional processes (coral reef growth, Anthony, 2008), while marine terraces are mostly related to wave erosion processes and sedimentary deposition. In general, reef terraces are discussed within the framework of keep-up/catch-up/give-up (Neumann and Macintyre, 1985) and backstepping processes (Woodroffe and Murray-Wallace, 2012), and they usually range from few hundred meters to 1-2 kilometers in width (Figure 7a). The possibility to date corals preserved on the terrace surface using U-series (^{230}Th/U) methods (e.g. Muhs et al., 1994; Stirling et al., 1998) has resulted in the widespread use of coral reef terraces as sea-level indicators, especially in uplifting areas (such as Barbados or Papua New Guinea, Bard et al., 1990; Chappell et al., 1996; Schellmann et al., 2004) where coralline stair-stepped landscapes are preserved (Kelsey, 2015).

In general, paleo RSL is determined from the average elevation of the terrace or, if present, from the elevation of the highest *in situ* corals which are usually found on the paleo reef crest. Considerations of the water-depth range of different coral species, or the occurrence of particular benthic assemblages or growth forms with a limited living range (e.g., such as microatolls which are constrained to the intertidal zone, Woodroffe et al., 2012) can further improve paleo RSL estimates. A reef flat typically extends up to the mean lower low water (MLLW, Figure 6a), which represents the general upper limit of the living range of corals. The depth of the coral reef terrace is dependent on the hydrodynamic conditions it is exposed to. A modern reef flat is rarely observed deeper than 3 meters (Blanchon, 2011).

3.3 Shore platforms

Shore platforms (Figure 4c, Figure 7a,b) are sub-horizontal rocky surfaces that interrupt vertical or sub-vertical cliffs near sea-level (Kennedy, 2015). Shore platforms have been classically divided in two categories: those sloping gently between about 1° and 5°, and those which are horizontal (Sunamura, 1992; Trenhaile, 1987). To these two types, Bird, 2011 added structural shore platforms, which are found where waves have exposed the surface of a flat or gently dipping resistant rock formation, usually a bedding plane. Shore platforms can be characterized by a number of smaller scale features such as wave ramps, potholes and other abrasion forms created by wave action, bioerosion, and/or chemical erosion (Figure 7f). Although the terms ‘shore platform’ and ‘marine terrace’ have been often used as synonyms, we highlight that they indicate different landforms. One of the main differences resides in the width scale: few tens of meters for shore platforms, few hundreds of meters to kilometers for marine terraces (see scale bars in Figure 4a,c). Another important difference is that, often, a shore platform represents an exposed rock surface, while a marine terrace is often covered by coastal or marine deposits.

The contact point between the horizontal bedrock and the vertical rocky cliff (i.e. the inner margin) is usually considered a good paleo RSL indicator, and shore platforms have been used as RSL indicators in a number of settings (Figure 7c,d,e). Nevertheless, disagreement exists as to whether marine or sub-aerial processes play the major role in shaping shore platforms (Trenhaile and Kanyaya, 2007; Trenhaile and Porter, 2007; Trenhaile, 2008; Stephenson and Kirk, 2000; Gómez-Pujol et al., 2015; Stephenson, 2000). The amplitude of the tidal range is considered to be significant as it determines the height of wave attack as well as the kind of waves reaching the platform, factors which can influence both weathering and

biological activities (Kanyaya and Trenhaile, 2005). To be more exact, the initiation and evolution of a shore platform depends on a balance between the geological properties of the bedrock and the coastal environmental forcing (Gómez-Pujol et al., 2006; Kennedy and Dickson, 2006; Naylor and Stephenson, 2010). Wave energy appears to play a significant role, with sloping platforms formed in environments characterized by higher wave energy than horizontal platforms.

Following the above, the use of shore platforms as sea-level indicators must be informed by an understanding of the processes active in their development (Pirazzoli, 1996). In fact, while some platforms are carved above sea-level, others are initiated in intertidal to slightly subtidal zones. According to Kennedy, 2015 '*the seaward edge of a shore platform is defined as: the point where active erosion of the bedrock ceases*'. In general, the limits of the indicative range associated with shore platforms vary from mean higher high water (MHHW) to a point that, according to the above definition of Kennedy, 2015, lies between the mean lower low water (MLLW) and the breaking depth of significant waves. A first-order estimate of the lower limit of a shore platform can be the midpoint between these two depths (Figure 4c).

3.4 Beach deposits and beach rocks

Beaches are loose accumulations of sand, gravel or pebbles that characterize many coasts worldwide (Anthony, 2005). The upper limit of a beach is on land while its lower limit is typically found in the upper subtidal zone (Figure 4d). Cemented beach deposits have been used as RSL indicators in a number of MIS 5e studies (see sup. mat. in Pedoja et al., 2014), but very few of these studies consider their vertical range of formation in the calculation of the paleo RSL (see example for the cemented beach deposit in Cala Millor, Figure 15).

There are several potential ways to define the upper and lower limits of a beach (Short, 1999; Chrzastowski, 2005). As an example, the beach can range from the wave base (often located at -10 to -30m depth) to the toe of the dune (several meters above sea-level). Here we consider that a beach is limited offshore by the longshore bar (located at the breaking depth, d_b), and onshore by the ordinary berm (ob). These two features can be up to 1 km apart. More exact sea-level information might be derived from sedimentary structures that are related to particular zones within the beach (Figure 8). For example, keystone vugs or beach fenestrae (Dunham, 1970) are formed as air bubbles are trapped in fine sand when inundated by sheets of water (Hearty et al., 1998), and thus typically indicate an environment between mean sea-level and the mean higher high tide (MHHW). On the other hand, the contact between subtidal and intertidal beach beds characterizes an environment close to the mean lower low tide (MLLW). A detailed account of beach structures that might be used for paleo sea-level studies is contained in Tamura, 2012 (their Fig.6).

While fossil beach deposits may be composed of loose sediments sometimes slightly cemented, beachrocks are lithified coastal deposits (Figure 4e, Figure 9a,b) that are organized in sequences of slabs with seaward inclination generally between 5° and 15° (Desruelles et al., 2009; Vacchi et al., 2012). Lithification is '*a function of CO_3^{-2-} ion concentration in seawater, microbial activity and degassing of CO_2*

from seaward flowing groundwater' (Mauz et al., 2015). In other words, beachrock forms in a mixing zone at the interface between seawater and meteoric water (see Mauz et al., 2015, their Fig.2).

Although the utility of beachrock as a sea-level indicator has been debated (Kelletat, 2007; Knight, 2007), beachrocks have often been used as indicators for Last Interglacial sea-level (e.g O'Leary et al., 2008; Ramsay and Cooper, 2001; Sherman et al., 1993). In general, beachrock forms in a coastal environment between the upper shoreface, also defined as the surf zone, and the spray zone (Mauz et al., 2015). The upper shoreface (or surf zone) can be defined as the portion of the seafloor that is shallow enough to be agitated by everyday wave action, and usually corresponds to the breaking depth (d_b) of the significant wave height in the studied area over the longest possible recording period. In coastal engineering, the significant wave height (often indicated as SWH or Hs) is the mean wave height of the highest third of the waves over a defined period.

The sea-level information from beachrock deposits can be improved if information on cement fabric, mineralogy, and sediment bedding structures are reported (Vieira et al., 2007; Mauz et al., 2015). As an example, irregularly distributed needles of aragonite, isopachous fibers of aragonite, or isopachous aragonitic rims (bladed or fibrous) as well as micritic high-magnesium-calcite cement or small-scaled trough cross stratification can all constrain the indicative range to the lower intertidal zone (see Mauz et al., 2015, their Table 5 and Figure 2).

3.5 Beach ridges

The broadest definition of beach ridges is the one given by Otvos, 2000, who defined them as '*stabilized, relict intertidal and supratidal, eolian and wave-built shore ridges that may consist of either siliciclastic or calcareous clastic matter of a wide range of clasts dimensions from fine sand to cobbles and boulders*'. Although aeolian beach ridges may be used to reconstruct paleoenvironments (Hesp, 1984) and can define the terrestrial limits to sea-level (Mauz et al., 2013), wave-built beach ridges (Figure 4f, Figure 10a, b) can be used as last interglacial RSL indicators (e.g., Nichol, 2002; Schellmann and Radtke, 2010).

Wave-built ridges are created by accumulation of sediments on the upper part of the shoreline, and indicate sea-level with a broad indicative range, one that is limited in the seaward direction by the base of the ordinary berm (ob) and in the landward direction by the maximum ingression of storm waves (storm wave swash height, SWSH, Kelsey, 2015; Tamura, 2012). More precise sea-level reconstruction can be obtained from specific sedimentary structures or biological indicators within the beach ridge, but usually beach ridges can be regarded as low-quality sea-level indicators. Nevertheless, in some regions (e.g. Patagonia, Schellmann and Radtke, 2010), beach ridges are the only MIS 5e sea-level indicators available (Ribolini et al., 2011). Tamura, 2012 observes that it is particularly important to analyze the modern counterparts of relict beach ridges, in order to identify their characteristic elevation range and apply this range to paleo sea-level reconstructions in the same region.

3.6 Lagoon deposits

Lagoons are inland water bodies with continuous or intermittent connection to the open sea (Kjerfve, 1994). Lagoonal deposits typically consist of silty and clayey sediments, frequently characterized by the

presence of brackish or marine water fauna (Figure 4g). Usually, lagoon sediments are horizontally laminated (Zecchin et al., 2004) and may be interrupted by one or more sandy layers (possibly with fragments of marine shells) that represent the transport, into the lagoon, of storm deposits.

Normally the indicative range of a coastal lagoon is constrained between the mean lower low tide (MLLW) and the depth of the lagoon (dl) (Figure 11a). In Figure 11b,c we show that the depth of several lagoons worldwide (see Supplementary Data) averages at 2±1.5m, although some lagoons can reach down to -8m depth (Figure 11b, c). The stratigraphic context and living range of fossil fauna can further inform sea-level information from lagoonal sequences.

In general, the sea-level information yielded by paleo lagoon deposits is improved when they contain fossil *in situ* fauna, such as articulated bivalves or remnants of reefs built by bioconstructors. Several species of serpulids are known as primary builders that form reef-like structures with calcareous tubes that grow vertically on the substrate. Often these structures form in clumps and become cemented to each other (Ten Hove, 1979). Large serpulid reefs are today found in quiet, enclosed embayments and/or in brackish estuaries and lagoons (Bianchi et al., 1995; Fornós et al., 1997; Schwindt et al., 2004; Ten Hove and Weerdenburg, 1978). In addition, lagoonal facies are often characterized by foraminiferal and ostracod assemblages dominated by marine or brackish taxa (Debenay et al., 2000). All these biological features, if found in the fossil record, may serve to narrow the indicative range (Murray-Wallace et al., 1999).

3.7 Cheniers

Chenier ridges (cheniers, Figure 4g) can be defined as '*sandy or shelly ridges, differentiated from other sand or shell beach ridges by the fact that they are perched on and separated laterally from other cheniers on a chenier plain, by fine-grained, muddy (or sometimes marshy) sediments*' (The 'Encyclopedia of Coastal Science', Schwartz, 2005). More simply, cheniers are land strips separating different sections of a coastal lagoon (Figure 12b). Coarser sediments can accumulate on cheniers from over-washing of storm waves. With regards their dimensions, cheniers can be up to 6 m high (Figure 12a, b), tens of kilometers in length and hundreds of meters wide (Schwartz, 2005).

As they develop in near shore environments, cheniers can be used as sea-level indicators (Carlston, 1950; Trowbridge, 1954), but their precision is low unless additional stratigraphic information is present. In general, the indicative range of a chenier is from the mean higher high water (MHHW) to the top elevation of the feature, above MHHW. In general, the best guideline to the relationship between a paleo chenier and paleo RSL is given by observations of the distribution of modern cheniers in a region.

3.8 Tidal notches

Tidal notches (Figure 4i) are indentations or undercuttings (Figure 13a, b), a few centimetres to several meters deep, cut into rocky coasts by processes acting in the tidal zone (such as tidal wetting and drying cycles, bioerosion, or mechanical action). Tidal notches are shaped by the interplay of bioerosion, wave action and tidal wetting and drying cycles on limestone coasts (Antonioli et al., 2015; Carobene, 2014; Pirazzoli, 1996). The shape and preservation of tidal notches depends on the duration of the highstand:

as a notch can be formed in few hundreds of years, a prolonged highstand might result in cliff retreat and the undercutting of ever new surfaces.

Tidal notches are shaped near Mean Sea-level (MSL) on calcareous cliffs and their highest elevation is constrained by local tides, while their depth (i.e. how deep they are cut into the rocky cliff) is related to intensity of local waves, bioerosion agents and presence of waters undersaturated of calcium carbonates (e.g. freshwater springs, Antonioli et al., 2015). MSL usually corresponds to the point of maximum concavity of the notch (Figure 13c, f). The height of the notch is always less than extreme tide values, and instead typically falls between mean higher high water (MHHW) and mean lower low water (MLLW).

Tidal notches formed during the Last Interglacial have been used as RSL indicators in several locations (Antonioli et al., 2006; Carobene, 2014; Hearty et al., 2007). They are especially effective sea-level indicators in regions with a low tidal range (such as the Mediterranean sea), where they can indicate sea-level with a precision of few decimetres (Figure 13d,e). The sea-level information can be even more precise if biological indicators, such as traces left by bioerosional organisms near MLLW (Laborel and Laborel-Deguen, 1996; Rovere et al., 2015a) have been preserved in the notch. While such bioerosonal remains can be used to date Holocene notches, MIS 5e biological assemblages associated with tidal notches are very rare. The main limitation on the use of tidal notches as MIS 5e RSL indicators is therefore that they can be hardly dated directly—their age can only be derived from chronostratigraphic correlations with other RSL indicators, such as beach or lagoonal deposits found in proximity to the notch.

3.9 Abrasion notches and sea caves

Abrasion processes are active where sand, gravel or pebbles are thrown against the rock by incoming waves resulting in erosion of a rocky shore face. This process creates abrasion notches (Figure 14a, b) that usually span a larger vertical distance than tidal notches. They also occur in all lithologies (while tidal notches occur only on carbonate rocks). As the formation of abrasion notches occurs where sediments can be mobilized by waves, abrasion notches have a large indicative range reaching from the storm swash wave height to the breaking depth of significant waves.

Coastal caves can be classified according to whether they are submerged or subaerial (Ferranti, 1998). Submerged caves originally formed in continental environments above sea-level and were later drowned by a relative sea-level rise. The largest submerged caves are formed by karst dissolution of the landscape. Other caves of continental origin include, for example, volcanic caves (Cicogna et al., 2003). One of the most widely recognized examples of submerged (karst) caves are blue holes on carbonate banks (Mylroie et al., 1995). Other examples of submerged karst caves can be found along the coastlines of central and southern Italy (Ferranti, 1998) or Croatia (Surić et al., 2009a, b). In his review of underwater cave systems in carbonate rocks, Ferranti, 1998 argues that, in the absence of further paleo RSL indicators, karst caves are an imprecise sea-level indicator.

Subaerial coastal caves, on the other hand, form near sea-level by mechanical abrasion processes (Colantoni, 1976). In general, this kind of cave displays an elongated shape, narrowing towards the interior, resulting in a short, wedge-shaped section orthogonal to the shore and a triangle or trapezium-shaped section parallel to the coastline (Ferranti, 1998). Coastal caves usually form along structural

weaknesses in the bedrock (faults, joints, strata) and bioerosion and chemical dissolution are important processes in carving the cave, especially along carbonate coastlines. While good sea-level indicators such as tidal notches or fixed biological indicators can be preserved in these caves (Carobene, 2014), typically it is the levelled floor at the entrance of the cave, often associated with abrasion notches, that provides a marker for RSL. This level represents the minimum level of constant wave action, and its precision in indicating sea-level is comparable to that of abrasion notches, described above.

Finally, the use of deposits found inside marine caves is widespread in sea-level studies. Caves can effectively preserve deposits from marine erosion including beach deposits (Hearty et al., 1999) and archaeological indicators (e.g. in the Cosquer Cave, near Marseille, France, described by Lambeck & Bard, 2000). In addition, speleothems (Bard et al. 2002, Vesica et al., 2000) containing alternations of continental and marine layers have been used to reconstruct Pleistocene sea-level history (Antonioli & Oliverio, 1996; Antonioli et al., 2001, 2004; Dutton et al., 2009a,b; Vesica et al., 2000).

4. Dating methods

Together with the measurement and interpretation of the elevation of MIS 5e RSL indicators, it is essential to establish their age as precisely as possible with absolute or relative dating methods. Among the absolute dating techniques most often used in Last Interglacial studies, only ^{230}Th/U dating of corals can resolve timing of deposition within the interglacial (Dutton and Lambeck, 2012; O'Leary et al., 2013). Other techniques, such as electron spin resonance (ESR), optically stimulated and thermo luminescence (OSL and TL), can be used mostly to distinguish if the RSL indicators, or associated fossil remnants, were formed within MIS 5e, as opposed to other interglacials, leaving the establishment of the relative timing of deposition within MIS 5e to other stratigraphic considerations (e.g. Grün, 1989; Hearty and Kaufman, 2000).

The most widely used relative dating technique in MIS 5e studies is probably amino acid racemization (AAR). Other relative methods, such as biostratigraphy and chronostratigraphic correlations are also widely used in MIS 5e studies. In the absence of absolute chronological constraints, these age attributions can usually help to distinguish between different interglacials, but they cannot be used to give a precise age. Although a complete review of dating methods applied to MIS 5e shorelines is beyond the scope of this paper, Table 4 lists the absolute and relative methods used in MIS 5e studies with the typical uncertainty in the final age attribution.

5. Last Interglacial shorelines: an applied example

5.1 From field measurement to paleo RSL

As described in the previous sections, the most accurate way to calculate the paleo RSL associated with a MIS 5e deposit is to study its modern analog. An example of how studies and datasets on modern coastal dynamics can be used to derive the indicative meaning of a MIS 5e beach deposit is presented in Figure 15. The example is that of Cala Millor, Mallorca Island, Spain. Cala Millor is an ~1.7 km-wide sandy beach

(Figure 15a). The beach profile is bounded on its low end by the presence of a longshore bar (Figure 15a), which has been shown to be persistent throughout the year (Tintoré et al., 2009, 2013; Gómez-Pujol et al., 2011). On the upper part of the beach (above MSL), beach berms can form according to the wave conditions in the study area (Figure 15c). Depending on the season or on the intensity of storm events in a given period, the berms are found higher (usually in winter) or lower (usually in summer) on the shoreline, with their location being a function of the maximum wave runup.

In the southern part of the beach of Cala Millor (white dot in Figure 15a,b) we surveyed a fossil beach deposit containing the fossil *Strombus latus* (ex. *S. bubonius*). This fossil is widespread in Mediterranean MIS 5e deposits, and it is often used as a biostratigraphic age indicator (Ferranti et al., 2006). We measured the upper and lower elevation of the deposit with a DGPS equipped with Omnistar real-time differential corrections. The deposit respectively 1.47±0.02m and 0.97±0.03m above the EGM08-REDNAP geoid model, which closely approximates sea-level in Spain. The average of these two measurements represents the mean elevation of the paleo RSL indicator (1.22 m). The elevation error (E_e in Table 1) can be calculated as the sum of half of the range between the two values (0.25 m) and the two measurement errors (0.02 and 0.03 m). This results in an elevation for the RSL indicator of 1.22±0.30 m, Figure 15b).

From bathymetric data, we determine that the longshore bar in Cala Millor can be found at an average depth of -1.9 m (Figure 15e). We adopt this value as the lower limit of the indicative range. For the upper limit, we need to establish the average elevation where beach berms are formed in Cala Millor. On the 19th of February 2015, we measured wave heights (Figure 15c) using pressure sensors in the surf zone (Harris et al., 2015) and beach topography (Figure 15b) using structure-from-motion techniques from drone (Casella et al., 2014, 2016). From these data, we determined that an onshore wave height averaging 0.6 m created a beach berm at +0.8 m (height of the maximum run-up shown on Figure 15c,d). As the swell we measured is roughly representative of the average swells in the area (Gómez-Pujol et al., 2011), we adopt as an upper limit of our IR the measured value the measured elevation of the berm.

Using the depth of the longshore bar (-1.9 m) and the calculated elevation of the ordinary berm (+0.8 m) as respectively lower and upper limits of the indicative range, we can apply Eqs. 1-4 (Table 1) to calculate the paleo RSL for Cala Millor. The calculated paleo RSL is 1.8±1.4 m (Figure 15e). The large uncertainty comes from the fact that, despite using precise measuring techniques, the beach deposit has a large indicative range and is therefore a relatively poor sea-level indicator. The indicative range might be reduced, for example, by investigating patterns in the cement of the lithified beach. It is worth highlighting that the paleo RSL calculated in this example matches, although with large uncertainties, the more precise elevation of MIS 5e paleo RSL inferred by measuring and dating phreatic overgrowths on speleothems inside Cova des Serral (Vesica et al., 2000), located few kilometers from this study site. The speleothem represents in fact a paleo RSL at +1.5m (no uncertainties reported) dated with ^{230}Th/U at 121.3±5.6 ka (see blue band Figure 15e).

Coupling research on paleo sea-levels with that on modern coastal dynamics is not always straightforward. Taking the above example of a beach deposit, the upper and lower limits of the indicative range depend strongly on the wave regime in the area of interest, a regime that can evolve over time. For instance, in the Bahamas, the Last Interglacial may have been characterized by storms of higher intensity than modern ones (Hearty et al., 1998; Tormey, 2007; Hansen et al., 2015). If true, then a beach deposit in the Bahamas should be characterized by a broader indicative range than a modern one.

5.2 From paleo RSL to long-term tectonics

The elevation of the Last Interglacial shoreline is often used as a benchmark for long-term tectonics (e.g. Guillaume et al., 2013), which is in turn used, for example, to plan coastal infrastructures or evaluate coastal risks. In most literature attempting to calculate long-term tectonics from sea-level data, if the MIS 5e shoreline is between 3 and 7 meters above present, it is assumed that a coastal region is tectonically stable in the long-term, especially if it is located on a passive margin. This view arises from the assumption that the elevation of MIS 5e eustatic sea-level was ~5m above present and that there is no GIA disequilibrium between the past interglacial and present one. However, Creveling et al., 2015, showed that when calculating long-term tectonics from MIS 5e shorelines, one must take into account the departures from eustasy due to GIA in response to glacial-interglacial cycles as well as excess polar ice-sheet melt relative to present day values.

Therefore, to calculate the tectonic displacement of a MIS 5e shoreline it is necessary to know the elevation of the paleo RSL (as calculated for Cala Millor in the section above), together with the elevation of eustatic sea-level (ESL) and the amount of glacio-hydro-isostatic (GIA) disequilibrium since the marker was deposited. Hereafter, we follow-up on the example given in previous section and show how the influence of tectonics can be evaluated using the Eqs. 5a, 6 and 8 (Table 1).

First, we calculate two different ESL scenarios for MIS 5e using a 410kyr-long global ice-sheet model (ANICE, a 3D thermo-mechanical ice-sheet model, de Boer et al., 2014). The first represents a two-step highstand with Greenland contributing 2.0 m of ESL equivalent between 127 and 116 ka, while Antarctica contributes 5.0 m but only after 120 ka (Figure 16a). This is in line with the scenario proposed by O'Leary et al., 2013. The second scenario reflects a more classical view of MIS 5e sea-level history, with melting of both Greenland (2.0m) and Antarctica (5.0m) happening early in the interglacial and ESL not changing until insolation in both hemispheres decreases and glacial conditions emerge (Figure 16b). These represent only two possible MIS 5e sea-level histories (compare with Kopp et al., 2009, Figure 16e). For each of these ESL scenarios, we calculate the MIS 5e GIA and RSL history at Cala Millor, Mallorca (Figure 16c,d). This is done by coupling the ANICE model with SELEN, a GIA model (Spada and Stocchi, 2007). In order to explore the uncertainties of GIA predictions due to the mantle viscosity profile, we use three different viscosity models (see box in Figure 16 for details). The average of all GIA-ESL scenarios for the time frame 125-117 ka is 4.1±3.7 m.

Next, we use the model results described above and the RSL for Cala Millor (=1.8±1.4 m) as inputs to Eqs.6 and 8 (Table 1) to calculate the rate of post-depositional displacement since MIS 5e in Cala Millor. As the age of the deposit has been constrained only by biostratigraphy, we assume that it could have been formed at any time during the MIS 5e highstand, therefore T in Eq.6 and 8 spans from 125 to 117 ka, the time frame for which GIA and ESL models predict the highstand (see also Fig.15e). We determine that possible tectonic rates in this area are constrained between -0.02±0.03 m/ka (Figure 16f).

While Mallorca is usually considered to have been tectonically stable since MIS 5e (e.g. Dorale et al, 2010), our results show that stability, mild subsidence or mild uplift are all possible influences given uncertainty in GIA models, ESL scenarios and RSL observations. It is worth highlighting that this example shows only a small range among the possible ESL scenarios (Kopp et al., 2009, Figure 16e), GIA predictions (e.g. compare the three mantle viscosities shown here with the 36 different mid-Pliocene

earth models with varying mantle viscosities shown in Rovere et al., 2015b) and duration of the MIS 5e highstand. As more eustatic scenarios and Earth models are considered, the tectonic rate range shown in Figure 16f is likely to change. In general, we conclude that the assumption that Mallorca is tectonically stable in the long term is supported by the MIS 5e shoreline record, but with considerable uncertainty. This has direct implications for Holocene studies—if we assume that the rates calculated here (-0.02±0.03 m/ka) are constant trough time, a mid-Holocene RSL marker deposited at 5 ka in Mallorca could already have been displaced by -25 to +6 cm. This 31 cm range, albeit small, should be added to the uncertainties on the Holocene sea-level index points in this area. It is worth noting, in fact, that some Holocene sea-level indicators can have accuracies down to few decimeters (Vacchi et al., 2016) and therefore a variation in the range of 3 decimeters is not negligible.

6. Discussion

How did the polar ice sheets, and hence sea-level, respond to MIS 5e warm conditions? Last Interglacial RSL indicators are often used to infer paleo RSL at one location. In turn, observations at many sites can contribute to a global understanding how polar ice sheets responded to moderate climate warming. Despite the long tradition of MIS 5e studies, often the methods used to measure the markers are not sufficiently described, are of low accuracy, or are not referred to a known tidal datum. Additionally, in many cases the measurement and interpretation are not clearly disentangled, making it virtually impossible to understand how the paleo RSL was derived, and assumptions of post-depositional vertical movements are often circular, not taking into account the effect of GIA disequilibrium since the LIG (Figure 16).

All of these factors contribute to discrepancies in MIS 5e sea-level reconstructions despite the fact that these sea-level indicators have been studied at hundreds of sites worldwide (Dutton and Lambeck, 2012; Kopp et al., 2009; Pedoja et al., 2014, 2011a). Early studies concluded that sea-level during MIS 5e was 3-6 m higher than today (Harmon et al., 1981; Neumann and Hearty, 1996; Stearns, 1976; Stirling et al., 1998) but none of these studies factored in the subsequent displacement of the field sites caused by glacial isostatic adjustment (GIA) which is now recognized as an important post-depositional process capable of biasing sea-level reconstructions (Lambeck and Nakada, 1992; Milne and Mitrovica, 2008; Potter and Lambeck, 2004). Recent studies by Kopp et al. (2009) and Dutton and Lambeck (2012) analyzed global datasets of MIS 5e sea-level indicators and, after accounting for tectonics and GIA, concluded that the maximum eustatic (i.e., globally averaged) sea-level (ESL) was higher than previously thought, between +5 and +9.4 m above modern sea-level.

Uncertainty also surrounds the question of whether rapid century to millennial-scale oscillations in ESL occurred within MIS 5e. Field evidence from Bahamas (Chen et al., 1991; Hearty and Neumann, 2001; Hearty et al., 2007; Thompson et al., 2011), Yucatan (Blanchon et al., 2009), Western Australia (Eisenhauer et al., 1996; O'Leary et al., 2013), and the Aldabara Atoll (Braithwaite et al., 1973) suggest that sea-level may not have been uniform throughout MIS 5e and that a rapid sea-level rise happened at the end of the interglacial. These studies support the hypothesis that, after a period when sea-level remained relatively stable at ~+3-4m from the beginning of the interglacial, a sudden melting occurred at ~120 ka coinciding with maximum spring-summer insolation in the Southern Hemisphere (>60°S). This inferred melting caused the sea-level to rise up to ~9m. The results of Kopp et al., 2013 do not exclude

the possibility of ESL oscillations during MIS 5e (Figure 16e), while Dutton and Lambeck, 2012 invoke GIA overprinting as the reason for an apparent late MIS 5e sea-level rise at some of the sites mentioned above, especially those in the Caribbean region. In the Seychelles, where GIA effects are considered minimal, Dutton et al., 2015 show that between 125 and 130 ka the eustatic sea-level reached its maximum elevation at ~+7m, early in the interglacial.

The controversy that exists over the shape of the MIS 5e sea-level curve stems from discrepancies in field data and is in part caused by the fact that MIS 5e sea-level markers often have a wide indicative range. This undermines our ability to understand sea-level variability in a slightly warmer world, with obvious implications for the future. If a late, rapid ESL rise occurred during MIS 5e, then we might surmise that the dual climatic effects of a) ~8 ka of interglacial warmth penetrating the surface layers of the ocean, and b) local southern hemisphere summer insolation intensity approaching a maximum, could have been instrumental in leading to the rapid collapse of a significant additional fraction of the Antarctic polar ice sheets (as much as 6 m sea-level equivalent), possibly including sectors of the East Antarctic Ice Sheet. This possibility eerily mirrors recent reports by Joughin et al., 2014 and Rignot et al., 2014 suggesting that a runaway collapse of the West Antarctic Ice Sheet may already be underway, ~8 ka into the Holocene interglacial interval and at a time of near maximum southern hemisphere summer insolation.

7. Conclusions

Although MIS 5e is the most studied period of the Earth's past, at least in terms of paleo sea-level, much research still need to be directed towards obtaining better paleo RSL elevations from field data. In this review we addressed all the relevant observations that are needed when studying MIS 5e RSL markers. Most of the concepts reviewed here can also be applied to other interglacials. In conclusion, we highlight the following points:

- **Measurement.** The measured elevation of a RSL indicator should be surveyed with the maximum possible accuracy and referred to a known sea-level datum. An elevation measurement must always carry an uncertainty, as well as a description of how the uncertainty was calculated. The measured elevation can be updated (for instance, if better measurement techniques become available) but it represents the most fundamental sea-level information, therefore its longevity must be ensured. The location on the landform where the measurement was taken should also be precisely described.
- **Interpretation.** For any RSL indicator surveyed in the field a correct indicative meaning, composed of an Indicative Range (IR) and a Reference Water Level (RWL), must be given. These values allow the reconstruction of the paleo RSL, which is the only observation that can be used to constrain GIA, other land movements, or ESL. As estimates of IR and RWL might be improved as new techniques or more detailed analyses are carried out, it is necessary that these parameters are reported separately from the measured elevation of the RSL indicator.
- **Modern analog.** In order to estimate the indicative meaning correctly, ancillary research on modern analogs should always be reported alongside the research on paleo landforms. At the same time, consideration must be given to the possible differences in environmental conditions between the time of formation of RSL indicators and the present. If surveys of the

modern analog are not possible, it is necessary to estimate IR and RWL using available literature data, or by inferring the general upper and lower bounds of similar landforms in the modern setting.

- **Age.** The information on RSL indicators (elevation, IR, RWL) should be always accompanied by information on how the age has been determined. If radiometric ages are available, it is necessary to indicate not only the final age, but all the analytical measurements that were used to define it. Each sample within the same site should carry its own positioning information (latitude, longitude and elevation with uncertainty). It is important also to disentangle the concept of sample for dating from that of RSL indicator: in Figure 1, we show an example where dating is derived from corals, but the RSL indication is obtained from the nearby terrace inner margin.
- **Tectonics.** Different possible ESL histories, glacial isostatic adjustment effects, uncertainty in age, and uncertainties in the paleo RSL reconstruction should always be included in tectonic calculations. The tectonic stability of an area should be evaluated on the basis of data that are independent from the MIS 5e sea-level marker.
- **Other vertical movements.** Together with crustal tectonics, it is necessary to consider all the other forces that can cause uplift or subsidence of a MIS 5e shoreline. Among these, sediment isostasy (Dalca et al., 2013) and earth dynamic topography (Müller et al., 2008; Moucha et al., 2008) are often overlooked, but are potentially relevant also along passive margins, that are usually considered 'stable' for which concerns MIS 5e histories. As an example, for the Atlantic Coast of the US, Rovere et al., 2014b estimated that dynamic topography can contribute to the uplift or subsidence of a MIS 5e shoreline from -0.25 to 3m, depending on where the shoreline is located along a North-South transect from North Carolina to Georgia. We remark that the amount of such displacements is equal to roughly the sea-level equivalent of a large part of the East Antarctic Ice Sheet.

Following these six points in the collection, analysis and reporting of field data will ensure their longevity and allow for their use in global compilations. In the supplementary material of this paper we propose the spreadsheet structure for building compilations of MIS 5e (and older) sea-level data, updating a formerly proposed one (Rovere et al., 2012). A similar approach applied to Holocene and Common Era sea-level reconstructions (Khan et al., 2015) has ensured that data collected by different research units are consistent and appropriate for use in global analyses of recent sea-level trends (Kopp et al., 2016).

Acknowledgments

AR's research is supported by the Institutional Strategy of the University of Bremen, funded by the German Excellence Initiative (ABPZuK-03/2014) and by ZMT, the Center for Tropical Marine Ecology. The authors acknowledge NSF grant OCE-1202632 'PLIOMAX' for support, as well as MEDFLOOD (INQUA CMP projects 1203P and 1603P) and PALSEA (PAGES/INQUA/WUN) working groups for useful discussions. MV contributes to the Labex OT-Med (n° ANR-11- LABX-0061) funded by the French Government «Investissements d'Avenir» program of the ANR through the A*MIDEX project (n° ANR-11-IDEX-0001-02). Data to build Fig. 15a were obtained from SOCIB (www.socib.es). The ideas in this review have been discussed with many colleagues, with whom separate papers have been published or are in

preparation: M. Aguirre (University of La Plata, AR); F. Antonioli (ENEA Rome, IT); K. Appeaning Addo (University of Ghana, GH); S. Avila (University of the Azores, PT); C.N. Bianchi (University of Genoa, IT); I. Castellanos (University of La Plata, AR); G. Cornamusini (University of Siena, IT); A. Droxler (Rice University, US); L. Ferranti (University of Napoli, IT); L. Foresi (University of Siena, IT); J.J. Fornos (University of Balearic Islands, ES); M. Firpo (University of Genoa, IT); B.P. Horton (Rutgers University, US); P. Jayson-Quashigah (University of Ghana, GH); T. Mann (ZMT Bremen, DE); T. Mensah-Senoo (University of Ghana, GH); M. Pappalardo (University of Pisa, IT); R. Ramalho (Bristol University, UK); D. Roberts (Council for Geosciences, SA); D. Sivan (University of Haifa, IL); G. Wiafe (University of Ghana, GH); and E. Zilbermann (Israel Geological Service, IL). We thank I. Candy, C. Murray-Wallace and another anonymous reviewer for insightful comments on a previous version of the MS.

References

Anthony, E.J., 2005. Beach erosion, in: Encyclopedia of Coastal Science. Springer, pp. 140–145.

Anthony, E.J., 2008. Shore processes and their palaeoenvironmental applications. Elsevier.

Antonioli, F. & Oliverio, M. 1996. Holocene Sea-Level Rise Recorded by a Radiocarbon-Dated Mussel in a Submerged Speleothem beneath the Mediterranean Sea. Quaternary Research, 45, 241-244.

Antonioli, F., Bard, E., Potter, E., Silenzi, S. & Improta, S. (2004). 215-ka History of sea-level oscillations from marine and continental layers in Argentarola Cave speleothems (Italy). Global and Planetary Change, 43, 57-78.

Antonioli, F., Ferranti, L., Kershaw, S., 2006. A glacial isostatic adjustment origin for double MIS 5.5 and Holocene marine notches in the coastline of Italy. Quat. Int. 145-146, 19–29.

Antonioli, F., Lo Presti, V., Rovere, A., Ferranti, L., Anzidei, M., Furlani, S., Mastronuzzi, G., Orru, P.E., Scicchitano, G., Sannino, G., Spampinato, C.R., Pagliarulo, R., Deiana, G., de Sabata, E., Sansò, P., Vacchi, M., Vecchio, A., 2015. Tidal notches in Mediterranean Sea: a comprehensive analysis. Quat. Sci. Rev. 119, 66–84.

Antonioli, F., Silenzi, S., Frisia, S. 2001. Tyrrhenian Holocene palaeoclimate trends from spelean serpulids. Quaternary Science Reviews, 20, 1661-1670.

Avila, S., Melo, C., Silva, L., Ramalho, R., Quartau, R., Hipolito, A., Cordeiro, R., Rebelo, A.C., Madeira, P., Rovere, A., Hearty, P.J., Henriques, D., da Silva, C.M., de Frias martins, A., Zazo, C., 2015. A review of the MIS 5e highstand deposits from Santa Maria Island (Azores , NE Atlantic): palaeobiodiversity , palaeoecology and palaeobiogeography. Quat. Sci. Rev. 114, 126–148. doi:10.1016/j.quascirev.2015.02.012

Bard, E., Antonioli, F., Silenzi, S. 2002. Sea-level during the penultimate interglacial period based on a submerged stalagmite from Argentarola Cave (Italy). Earth and Planetary Science Letters, 196, 135-146.

Bard, E., Hamelin, B., Fairbanks, R.G., 1990. U-Th ages obtained by mass spectrometry in corals from Barbados: sea-level during the past 130, 000 years. Nature 346, 456–458.

Bellucci, L.G., Frignani, M., Paolucci, D., Ravanelli, M., 2002. Distribution of heavy metals in sediments of the Venice Lagoon: the role of the industrial area. Sci. Total Environ. 295, 35–49.

Bianchi, C.N., Aliani, S., Morri, C., 1995. Present-day serpulid reefs, with reference to an on- going research project on Ficopomatus enigmaticus. Publ. du Serv. Geol. du Luxemb. 29, 61–65.

Bird, E., 2011. Coastal geomorphology: an introduction. John Wiley & Sons.

Blanchon, P., 2011. Geomorphic zonation. Encycl. Mod. Coral Reefs 469–486.

Blanchon, P., Eisenhauer, A., Fietzke, J., Liebetrau, V., 2009. Rapid sea-level rise and reef back-stepping at the close of the last interglacial highstand. Nature 458, 881–884.

Bonnet, D., Molinero, J.C., Schohn, T., Daly Yahia, M.N., 2012. Seasonal changes in the population dynamics of Aurelia aurita in Thau lagoon. Cah. Biol. Mar. 3, 343–347.

Braithwaite, C.J.R., Taylor, J.D., Kennedy, W.J., 1973. The evolution of an atoll: the depositional and erosional history of Aldabra. Philos. Trans. R. Soc. Lond. B. Biol. Sci. 307–340.

Bruneau, N., Fortunato, A.B., Dodet, G., Freire, P., Oliveira, A., Bertin, X., 2011. Future evolution of a tidal inlet due to changes in wave climate, Sea-level and lagoon morphology (Óbidos lagoon, Portugal). Cont. Shelf Res. 31, 1915–1930.

Buddemeier, R.W., Smith, S. V., Kinzie, R.A., 1975. Holocene windward reef-flat history, Enewetak Atoll. Bull. Geol. Soc. Am. 86, 1581–1584.

Carlston, C.W., 1950. Pleistocene history of coastal Alabama. Geol. Soc. Am. Bull. 61, 1119–1130.

Carobene, L., 2014. Marine Notches and Sea-Cave Bioerosional Grooves in Microtidal Areas : Examples from the Tyrrhenian and Ligurian Coasts — Italy 1–21. doi:10.2112/JCOASTRES-D-14-00068.1

Carr, A.S., Bateman, M.D., Roberts, D.L., Murray-Wallace, C. V, Jacobs, Z., Holmes, P.J., 2010. The last interglacial sea-level high stand on the southern Cape coastline of South Africa. Quat. Res. 73, 351–363.

Casella, E., Rovere, A., Pedroncini, A., Mucerino, L., Casella, M., Cusati, A.L., Vacchi, M., Ferrari, M., Firpo, M., 2014. Study of wave runup using numerical models and low-altitude aerial photogrammetry : A tool for coastal management. Estuar. Coast. Shelf Sci. 149, 160–167. doi:10.1016/j.ecss.2014.08.012

Casella, E., Rovere, A., Pedroncini, A., Stark, C.P., Casella, M., Ferrari, M., Firpo, M., 2016. Drones as tools for monitoring beach topography changes in the Ligurian Sea (NW Mediterranean). Geo-Marine Lett. doi:10.1007/s00367-016-0435-9

Chandana, E.P.S., Amarasinghe, N.J.D.S., Samayawardhena, L. a., 2008. Factors affecting the avi-faunal distribution in the three lagoons (Malala , Embillakala and Bundala Lewaya) of Bundala National Park (A Ramsar Wetland) in Sri Lanka. Ruhuna Jounal Sci. 3, 34–43.

Chappell, J., Omura, A., Esat, T., McCulloch, M., Pandolfi, J., Ota, Y., Pillans, B., 1996. Reconciliaion of late Quaternary sea-levels derived from coral terraces at Huon Peninsula with deep sea oxygen isotope records. Earth Planet. Sci. Lett. 141, 227–236.

Chen, J.H., Curran, H.A., White, B., Wasserburg, G.J., 1991. Precise chronology of the last interglacial period: 234U-230Th data from fossil coral reefs in the Bahamas. Geol. Soc. Am. Bull. 103, 82–97.

Choi, S.J., Merritts, D.J., Ota, Y., 2008. Elevations and ages of marine terraces and late Quaternary rock uplift in southeastern Korea. J. Geophys. Res. Solid Earth 113, 1–15. doi:10.1029/2007JB005260

Chrzastowski, M.J., 2005. Beach features, in: Encyclopedia of Coastal Science. Springer, pp. 145–147.

Cicogna, F., Bianchi, C.N., Ferrari, G., Forti, P. 2003. Le grotte marine: cinquant'anni di ricerca in Italia. Ministero dell'Ambiente e della Tutela del Territorio, Roma, 1-505.

Colantoni, P. 1976. Aspetti geomorfologici e genesi delle grotte sottomarine. Pubbl. Staz. Zool. Napoli, 40, 460-472.

Contreras Ruiz Esparza, A., Douillet, P., Zavala-Hidalgo, J., 2014. Tidal dynamics of the Terminos Lagoon, Mexico: Observations and 3D numerical modelling. Ocean Dyn. 64, 1349–1371.

Creveling, J.R., Mitrovica, J.X., Hay, C.C., Austermann, J., Kopp, R.E., 2015. Revisiting tectonic corrections applied to Pleistocene sea-level highstands. Quat. Sci. Rev. 111, 72–80. doi:10.1016/j.quascirev.2015.01.003

Dalca, A. V, Ferrier, K.L., Mitrovica, J.X., Perron, J.T., Milne, G.A., Creveling, J.R., 2013. On postglacial sea-level--III. Incorporating sediment redistribution. Geophys. J. Int. 194, 45–60.

Darwin, C., 1846. Geological observations on South America: being the third part of the geology of the voyage of the Beagle. Smith, Elder and Company.

De Boer, B., Stocchi, P., Van De Wal, R., 2014. A fully coupled 3-D ice-sheet-sea-level model: algorithm and applications. Geosci. Model Dev. 7, 2141–2156.

De Francesco, C.G., Isla, F.I., 2003. Distribution and abundance of hydrobiid snails in a mixed estuary and a coastal lagoon, Argentina. Estuaries 26, 790–797.

Dean, A.J., Steneck, R.S., Tager, D., Pandolfi, J.M., 2015. Distribution, abundance and diversity of crustose coralline algae on the Great Barrier Reef. Coral Reefs 34, 581–594.

Dias, J.M., Lopes, J.F., Dekeyser, I., 2001. Lagrangian transport of particles in Ria de Aveiro lagoon, Portugal. Phys. Chem. Earth, Part B Hydrol. Ocean. Atmos. 26, 721–727.

Dorale, J.A., Onac, B.P., Fornos, J.J., Gines, J., Gines, A., Tuccimei, P., Peate, D.W., 2010. Sea-Level Highstand 81,000 Years Ago in Mallorca. Science (80-.). 327, 860–863.

Dunham, R.J., 1970. Keystone Vugs in Carbonate Beach Deposits: ABSTRACT. Am. Assoc. Pet. Geol. Bull. 54, 845.

Düsterhus, A., Rovere, A., Carlson, A.E., Barlow, N.L.M., Bradwell, T., Dutton, A., Gehrels, R., Hibbert, F.D., Hijma, M.P., Horton, B.P., Klemann, V., Kopp, R.E., Sivan, D., Tarasov, L., Törnqvist, T.E., 2015. Palaeo sea-level and ice-sheet databases: problems, strategies and perspectives. Clim Past. 12(4), 911–921.

Dutton, A., Bard, E., Antonioli, F., Esat, T., Lambeck, K., McCulloch, M. 2009. Phasing and amplitude of sea-level and climate change during the penultimate interglacial. Nature Geosci, 2, 355-359.

Dutton, A., Lambeck, K., 2012. Ice volume and sea-level during the last interglacial. Science (80-.). 337, 216–219. doi:10.1126/science.1205749

Dutton, A., Scicchitano, G. et al. 2009. Uplift rates defined by U-series and 14C ages of serpulid-encrusted speleothems from submerged caves near Siracusa, Sicily (Italy). Quaternary Geochronology, 4, 2-10.

Dutton, A., Webster, J.M., Zwartz, D., Lambeck, K., Wohlfarth, B., 2015. Tropical tales of polar ice: evidence of Last Interglacial polar ice sheet retreat recorded by fossil reefs of the granitic Seychelles islands. Quat. Sci. Rev. 107, 182–196. doi:10.1016/j.quascirev.2014.10.025

Eisenhauer, A., Zhu, Z.R., Collins, L.B., Wyrwoll, K.H., Eichstätter, R., 1996. The Last Interglacial sea-level change: new evidence from the Abrolhos islands, West Australia. Geol. Rundschau 85, 606–614.

Engelhart, S.E., Horton, B.P., 2012. Holocene sea-level database for the Atlantic coast of the United States. Quat. Sci. Rev. 54, 12–25.

Engelhart, S.E., Horton, B.P., Douglas, B.C., Peltier, W.R., Tornqvist, T.E., 2009. Spatial variability of late Holocene and 20th century sea-level rise along the Atlantic coast of the United States. Geology 37, 1115–1118.

Falter, J.L., Lowe, R.J., Zhang, Z., McCulloch, M., 2013. Physical and Biological Controls on the Carbonate Chemistry of Coral Reef Waters: Effects of Metabolism, Wave Forcing, Sea-level, and Geomorphology. PLoS One 8.

Ferranti, L. 1998. Underwater cave systems in carbonate rocks as semi-proxy indicators of paleo-sea-levels. Il Quaternario - Italian Journal of Quaternary Sciences, 11(1), 41-52.

Ferranti, L., Antonioli, F., Mauz, B., Amorosi, A., Dai Pra, G., Mastronuzzi, G., Monaco, C., Orrù, P., Pappalardo, M., Radtke, U., Renda, P., Romano, P., Sansò, P., Verrubbi, V., 2006. Markers of the last interglacial sea-level high stand along the coast of Italy: Tectonic implications. Quat. Int. 145-146, 30–54.

Fornós, J.J., Forteza, V., Martínez-Taberner, A., 1997. Modern polychaete reefs in western Mediterranean lagoons: Ficopomatus enigmaticus (Fauvel) in the Albufera of Menorca, Balearic Islands. Palaeogeogr. Palaeoclimatol. Palaeoecol. 128, 175–186.

Foster, J., 2015. GPS and surveying, in: Shennan, I., Long, A.J., Horton, B.P. (Eds.), Handbook of Sea-Level Research. Wiley Online Library, pp. 157–170.

Gaki-Papanastassiou, K., Karymbalis, E., Papanastassiou, D., Maroukian, H., 2009. Quaternary marine terraces as indicators of neotectonic activity of the Ierapetra normal fault SE Crete (Greece). Geomorphology 104, 38–46. doi:10.1016/j.geomorph.2008.05.037

Galili, Zviely, Ronen, Mienis, 2007. Beach deposits of MIS 5e high sea stand as indicators for tectonic stability of the Carmel coastal plain, Israel. Quat. Sci. Rev. 26, 14.

Goatley, C.H.R., Bellwood, D.R., 2012. Sediment suppresses herbivory across a coral reef depth gradient. Biol. Lett. 8, 1016–8.

Gómez-Pujol, L., Cruslock, E., Fornós, J.J., Swantesson, J.O.H., 2006. Unravelling factors that control shore platforms and cliffs in microtidal coasts. Suppl. Vol. 44, 117-135.

Gómez-Pujol, L., Orfila, A., Álvarez-Ellacuría, A., Tintoré, J. 2011. Controls on sediment dynamics and medium-term morphological change in a barred microtidal beach (Cala Millor, Mallorca, Western Mediterranean). Geomorphology 132, 87-98.

Gómez-Pujol, L., Pérez-Alberti, A., Blanco-Chao, R., Costa, S., Neves, M., del Río, L., 2015. The rock coast of continental Europe in the Atlantic. In: Kennedy, D.M., Stephenson, W.J., Naylor, L.A. (Eds.), Rock Coast Geomorphology: A Global Synthesis. Geological Societym¡, London, Memoirs 40: 77-88.

Graciotti, R., Foresi, L.M., Pantaloni, M., 2002. Caratteristiche geomorfologiche dell'Isola di Pianosa (Arcipelago toscano). Atti Soc. toscana di Sci. Nat. Mem., Ser. A 108, 95–111.

Grün, R., 1989. Electron spin resonance (ESR) dating. Quat. Int. 1, 65–109.

Guillaume, M.M.M., Reyss, J.L., Pirazzoli, P.A., Bruggemann, J.H., 2013. Tectonic stability since the last interglacial offsets the Glorieuses Islands from the nearby Comoros archipelago. Coral Reefs 32, 719–726. doi:10.1007/s00338-012-1006-9

Hallermeier, R.J., 1981. A profile zonation for seasonal sand beaches from wave climate. Coast. Eng. 4, 253–277.

Hanna, A.J.M., Allison, M.A., Bianchi, T.S., Marcantonio, F., Goff, J.A., 2014. Late Holocene sedimentation in a high Arctic coastal setting: Simpson Lagoon and Colville Delta, Alaska. Cont. Shelf Res. 74, 11–24.

Hansen, J., Sato, M., Hearty, P., Ruedy, R., Kelley, M., Masson-Delmotte, V., Russell, G., Tselioudis, G., Cao, J., Rignot, E., others, 2015. Ice melt, sea-level rise and superstorms: evidence from paleoclimate data, climate modeling, and modern observations that 2◦ C global warming is highly dangerous. Atmos. Chem. Phys. Discuss. 15, 20059–20179.

Harmon, R.S., Land, L.S., Mitterer, R.M., Garrett, P., Schwarcz, H.P., Larson, G.J., 1981. Bermuda sea-level during the last interglacial. Nature 289, 481–483.

Harris, D.L., Vila-Concejo, A., Webster, J.M., Power, H.E., 2015 Spatial variations in wave transformation and sediment entrainment on a coral reef sand apron. Mar Geol. 363,220–229.

Hearty, P., 1987. New data on the Pleistocene of Mallorca. Quat. Sci. Rev. 6, 245–257.

Hearty, P.J., 2002. Revision of the late Pleistocene stratigraphy of Bermuda. Sediment. Geol. 153, 1–21.

Hearty, P.J., Hollin, J.T., Neumann, a. C., O'leary, M.J., McCulloch, M., O'Leary, M.J., 2007. Global sea-level fluctuations during the Last Interglaciation (MIS 5e). Quat. Sci. Rev. 26, 2090–2112. doi:10.1016/j.quascirev.2007.06.019

Hearty, P.J., Kaufman, D.S., 2000. Whole-Rock Aminostratigraphy and Quaternary Sea-Level History of the Bahamas. Quat. Res. 54, 163–173.

Hearty, P.J., Neumann, A.C., 2001. Rapid sea-level and climate change at the close of the Last Interglaciation (MIS 5e): evidence from the Bahama Islands. Quat. Sci. Rev. 20, 1881–1895.

Hearty, P.J., Neumann, A.C., Kaufman, D.S., 1998. Chevron ridges and runup deposits in the Bahamas from storms late in oxygen-isotope substage 5e. Quat. Res. 50, 309–322.

Hearty, P.J., Vacher, H.L., Mitterer, R.M., 1992. Aminostratigraphy and ages of Pleistocene limestones of Bermuda. Geol. Soc. Am. Bull. 104, 471–480.

Hesp, P. 1984. Foredune formation in Southeast Australia. In: B.G. Thom (Ed), Coastal Geomorphology in Australia, pp.69-97, Academic Press, Sydney.

Hibbert, F., Zhao, C., Rohling, E., Williams, F., 2014. Coral and speleothem records of past sea-level change: a global repository, in: EGU General Assembly Conference.

Hijma, M.P., Engelhart, S.E., Törnqvist, T.E., Horton, B.P., Hu, P., Hill, D.F., 2015. A protocol for a geological sea-level database. Handb. Sea-Level Res. 536–553.

Hutton, F.W., 1885. Sketch of the geology of New Zealand. Q. J. Geol. Soc. 41, 191–220.

Huybrechts, P., Gregory, J., Janssens, I., Wild, M., 2004. Modelling Antarctic and Greenland volume changes during the 20th and 21st centuries forced by GCM time slice integrations. Glob. Planet. Change 42, 83–105.

IPCC, Stocker, T.F., Qin, D., Plattner, G.-K., Tignor, M., Allen, S.K., Boschung, J., Nauels, A., Xia, Y., Bex, V., Midgley, P.M., 2013. Climate Change 2013. The Physical Science Basis. Working Group I Contribution to the Fifth Assessment Report of the Intergovernmental Panel on Climate Change-Abstract for decision-makers.

Jokiel, P.L., Rodgers, K.S., Storlazzi, C.D., Field, M.E., Lager, C. V., Lager, D., 2014. Response of reef corals on a fringing reef flat to elevated suspended-sediment concentrations: Moloka'i, Hawai'i. PeerJ 2, e699.

Joughin, I., Smith, B.E., Medley, B., 2014. Marine Ice Sheet Collapse Potentially Under Way for the Thwaites Glacier Basin, West Antarctica. Science (80-.). 344, 735–738.

Juggins, S., Birks, H.J.B., 2012. Quantitative environmental reconstructions from biological data, in: Tracking Environmental Change Using Lake Sediments. Springer, pp. 431–494.

Kanyaya, J.I., Trenhaile, A.S., 2005. Tidal wetting and drying on shore platforms: An experimental assessment. Geomorphology 70, 129–146.

Kattsov, V.M., Källén, E., Cattle, H.P., Christensen, J., Drange, H., Hanssen-Bauer, I., Jóhannesen, T., Karol, I., Räisänen, J., Svensson, G., 2005. Future climate change: Modeling and scenarios for the Arctic.

Kelletat, D., 2007. Reply to: KNIGHT, J., 2007. Beachrock Reconsidered. Discussion of: KELLETAT, D., 2006. Beachrock as Sea-Level Indicator? Remarks from a Geomorphological Point of View, Journal of Coastal Research, 22(6), 1558–1564; Journal of Coastal Research, 23(4), 1074. J. Coast. Res. 236, 1605–1606.

Kelsey, H.M., 2015. Geomorphological indicators of past sea-levels, in: Handbook of Sea-Level Research. pp. 66–82.

Kench, P.S., Brander, R.W., 2006. Wave Processes on Coral Reef Flats: Implications for Reef Geomorphology Using Australian Case Studies. J. Coast. Res. 221, 209–223.

Kennedy, D.M., 2015. Where is the seaward edge? A review and definition of shore platform morphology. Earth-Science Rev. 147, 99–108. doi:10.1016/j.earscirev.2015.05.007

Kennedy, D.M., Dickson, M.E., 2006. Lithological control on the elevation of shore platforms in a microtidal setting. Earth Surf. Process. Landforms 31, 1575–1584.

Kern, J.P., 1977. Origin and history of upper Pleistocene marine terraces, San Diego, California. Geol. Soc. Am. Bull. 88, 1553–1566.

Kharroubi, A., Gzam, M., Jedoui, Y., 2012. Anthropogenic and natural effects on the water and sediments qualities of costal lagoons: Case of the Boughrara Lagoon (Southeast Tunisia). Environ. Earth Sci. 67, 1061–1067.

Kjerfve, B., 1994. Coastal lagoons. Elsevier Oceanogr. Ser. 60, 1–8.

Knight, J., 2007. Beachrock Reconsidered. Discussion of: Kelletat, D., 2006. Beachrock as Sea-Level Indicator? Remarks from a Geomorphological Point of View. Journal of Coastal Research,22(6), 1558–1564. J. Coast. Res. 234, 1074–1078.

Khan, N.S., Ashe, E., Shaw, T.A., Vacchi, M., Walker, J., Peltier, W.R., Kopp, R.E., Horton, B.P., 2015. Holocene Relative Sea-Level Changes from Near-, Intermediate-, and Far-Field Locations. Curr. Clim. Chang. Reports 1, 247–262. doi:10.1007/s40641-015-0029-z

Kopp, R.E., Kemp, A.C., Bittermann, K., Horton, B.P., Donnelly, J.P., Gehrels, W.R., Hay, C.C., Mitrovica, J.X., Morrow, E.D., Rahmstorf, S., 2016. Temperature-driven global sea-level variability in the Common Era. PNAS.

Kopp, R.E., Simons, F.J., Mitrovica, J.X., Maloof, A.C., Oppenheimer, M., 2013. A probabilistic assessment of sea-level variations within the last interglacial stage. Geophys. J. Int.

Kopp, R.E., Simons, F.J., Mitrovica, J.X., Maloof, A.C., Oppenheimer, M., 2009. Probabilistic assessment of sea-level during the last interglacial stage. Nature 462, 863–7. doi:10.1038/nature08686

Ku, T.-L., Kern, J.P., 1974. Uranium-series age of the upper Pleistocene Nestor terrace, San Diego, California. Geol. Soc. Am. Bull. 85, 1713–1716.

Laborel, J., Laborel-Deguen, F., 1996. Biological indicators of Holocene sea-level and climatic variations on rocky coasts of tropical and subtropical regions. Quat. Int. 31, 53–60.

Lambeck, K., Bard, E. 2000. Sea-level change along the French Mediterranean coast for the past 30000 years. Earth and Planetary Science Letters, 175, 203-222.

Lambeck, K., Nakada, M., 1992. Constraints on the age and duration of the last interglacial period and on sea-level variations. Nature 357, 125–128.

Lamptey, A.M., Ofori-Danson, P.K., Abbenney-Mickson, S., Breuning-Madsen, H., Abekoe, M.K., 2013. The Influence of Land-Use on Water Quality in a Tropical Coastal Area : Case Study of the Keta Lagoon Complex, Ghana, West Africa. Open J. Mod. Hydrol. 2013, 188–195.

Larson, M., Kraus, N.C., 1994. Temporal and spatial scales of beach profile change, Duck, North Carolina. Mar. Geol. 117, 75–94. doi:10.1016/0025-3227(94)90007-8

Lasagna, R., Albertelli, G., Colantoni, P., Morri, C., Bianchi, C.N., 2010. Ecological stages of Maldivian reefs after the coral mass mortality of 1998. Facies 56, 1–11.

Lee, G., Nicholls, R.J., Birkemeier, W.A., 1998. Storm-driven variability of the beach-nearshore profile at Duck, North Carolina, USA, 1981–1991. Mar. Geol. 148, 163–177. doi:10.1016/S0025-3227(98)00010-3

Lyell, C., 1837. Principles of geology: being an inquiry how far the former changes of the earth's surface are referable to causes now in operation. J. Kay, jun. & brother.

Lunt, D.J., Abe-Ouchi, A., Bakker, P., Berger, A., Braconnot, P., Charbit, S., Fischer, N., Herold, N., Jungclaus, J.H., Khon, V.C., Krebs-Kanzow, U., Langebroek, P.M., Lohmann, G., Nisancioglu, K.H., Otto-Bliesner, B.L., Park, W., Pfeiffer, M., Phipps, S.J., Prange, M., Rachmayani, R., Renssen, H., Rosenbloom, N., Schneider, B., Stone, E.J., Takahashi, E., Wei, W., Yin, Q., Zang, Z.S., 2013. A multimodel assessment of last interglacial temperatures. Climate of the Past 9, 699-717.

Macintyre, I.G., 1967. Submerged coral reefs, west coast of Barbados, West Indies. Can. J. Earth Sci. 4, 461–474.

Mann T., Rovere A., Schöne T., Klicpera A., Stocchi P., Lukman M., Westphal, H., 2016. The magnitude of a mid-Holocene sea-level highstand in the Strait of Makassar. Geomorphology 257, 155–63.

Mariath, R., Rodriguez, R.R., Figueiredo, M.A.O., 2013. Succession of crustose coralline red algae (Rhodophyta) on coralgal reefs exposed to physical disturbance in the southwest Atlantic. Helgol. Mar. Res. 67, 687–696.

Mauz, B., Hassler, U., 2000. Luminescence chronology of Late Pleistocene raised beaches in southern Italy: new data of relative sea-level changes. Mar. Geol. 170, 187–203.

Mauz, B., Hijma, M.P., Amorosi, A., Porat, N., Galili, E., Bloemendal, J., 2013. Aeolian beach ridges and their significance for climate and sea-level: Concept and insight from the Levant coast (East Mediterranean). Earth-Science Rev. 121, 31–54.

Mauz, B., Vacchi, M., Green, A., Hoffmann, G., Cooper, A., 2015. Beachrock: A tool for reconstructing relative sea-level in the far-field. Mar. Geol. 362, 1–16. doi:10.1016/j.margeo.2015.01.009

Mayer, R., Kriebel, D., 1994. Wave runup on composite-slope and concave beaches. Coast. Eng. Proc. 2325–2339.

Medina-Elizalde, M., 2013. A global compilation of coral sea-level benchmarks: Implications and new challenges. Earth Planet. Sci. Lett. 362, 310–318.

Meyers, J.H., 1987. Marine vadose beachrock cementation by cryptocrystalline magnesian calcite--Maui, Hawaii. J. Sediment. Res. 57.

Milne, G.A., Mitrovica, J.X., 2008. Searching for eustasy in deglacial sea-level histories. Quat. Sci. Rev. 27, 2292–2302.

Mongin, M., Baird, M., 2014. The interacting effects of photosynthesis, calcification and water circulation on carbon chemistry variability on a coral reef flat: A modelling study. Ecol. Modell. 284, 19–34.

Montaggioni, L.F., 2005. History of Indo-Pacific coral reef systems since the last glaciation: Development patterns and controlling factors. Earth-Science Rev. 71, 1–75.

Moucha, R., Forte, A.M., Rowley, D.B., Mitrovica, J.X., Simmons, N.A., Grand, S.P., 2008. Dynamic topography and long-term sea-level variations: There is no such thing as a stable continental platform. Geology 271, 101–108.

Müller, R.D., Sdrolias, M., Gaina, C., Steinberger, B., Heine, C., 2008. Long-term sea-level fluctuations driven by ocean basin dynamics. Science (80-.). 319, 1357–1362.

Muhs, D.R., Kennedy, G.L., Rockwell, T.K., 1994. Uranium-Series Ages of Marine Terrace Corals from the Pacific Coast of North America and Implications for Last-Interglacial Sea-level History. Quat. Res. 42, 72–87. doi:10.1006/qres.1994.1055

Muhs, D.R., Meco, J., Simmons, K.R., 2014. Uranium-series ages of corals, sea-level history, and palaeozoogeography, Canary Islands, Spain: An exploratory study for two Quaternary interglacial periods. Palaeogeogr. Palaeoclimatol. Palaeoecol. 394, 99–118.

Muhs, D.R., Rockwell, T.K., Kennedy, G.L., 1992. Late quaternary uplift rates of marine terraces on the pacific coast of North America , Southern Oregon to Baja California Sur. Quat. Int. 15, 121–133.

Muhs, D.R., Simmons, K.R., Schumann, R.R., Halley, R.B., 2011. Sea-level history of the past two interglacial periods: new evidence from U-series dating of reef corals from south Florida. Quat. Sci. Rev. 30, 570–590.

Muhs, D.R., Szabo, B.J., 1982. Uranium-series age of the Eel Point terrace, San Clemente Island, California. Geology 10, 23–26.

Muhs, D.R., Wehmiller, J.F., Simmons, K.R., York, L.L., 2004. Quaternary sea-level history of the United States, in: The Quaternary Period in the United States. Elsevier, pp. 147–183.

Mulvaney, R., Abram, N.J., Hindmarsh, R.C.A., Arrowsmith, C., Fleet, L., Triest, J., Sime, L.C., Alemany, O., Foord, S., 2013. Recent Antarctic Peninsula warming relative to Holocene climate and ice-shelf history. Nature 488, 141–144.

Murray-Wallace, C. V, Belperio, A.P., 1991. The last interglacial shoreline in Australia—a review. Quat. Sci. Rev. 10, 441–461.

Murray-Wallace, C. V., Woodroffe, C. D., 2014. Quaternary Sea-Level Changes - A Global Perspective, Cambridge University Press, Cambridge, 484 pp.

Mylroie, J.E., Carew, J.L., Moore, A.I. 1995. Blue holes: Definition and genesis. Carbonates Evaporites, 10, 225-233.

Nagasaka, M., Takano, M., 2014. Spatial and seasonal variability of turbidity in Lake Kahokugata, a shallow eutrophic lagoon in Japan, Lakes : The Mirrors of the Earth, BALANCING ECOSYSTEM INTEGRITY AND HUMAN WELLBEING.

Naylor, L.A., Stephenson, W.J., 2010. On the role of discontinuities in mediating shore platform erosion. Geomorphology 114, 89–100.

Neumann, A.C., Hearty, P.J., 1996. Rapid sea-level changes at the close of the last interglacial (substage 5e) recorded in Bahamian island geology. Geology 24, 775–778.

Neumann, A.C., Macintyre, I.G., 1985. Reef response to sea-level rise: Keep-up, catch-up or give-up. Int. Coral Reef Symp. 3, 105–110.

Nichol, S.L., 2002. Morphology, stratigraphy and origin of Last Interglacial beach ridges at Bream Bay, New Zealand. J. Coast. Res. 149–159.

Nichols, M.M., 1989. Sediment Accumulation Rates and Relative Sea-Level rise in Lagoons. Mar. Geol. 88, 201–219.

Nisi, M.F., Antonioli, F., Pra, G.D., Leoni, G., Silenzi, S., 2003. Coastal deformation between the Versilia and the Garigliano plains (Italy) since the last interglacial stage. J. Quat. Sci. 18, 709–721.

O'leary, M.J., Hearty, P.J., McCulloch, M.T., 2008. U-series evidence for widespread reef development in Shark Bay during the last interglacial. Palaeogeogr. Palaeoclimatol. Palaeoecol. 259, 424–435.

O'Leary, M.J., Hearty, P.J., Thompson, W.G., Raymo, M.E., Mitrovica, J.X., Webster, J.M., 2013. Ice sheet collapse following a prolonged period of stable sea-level during the last interglacial. Nat. Geosci. 6, 796–800. doi:10.1038/ngeo1890

O'Neal, M.L., Dunn, R.K., 2003. GPR investigation of multiple stage-5 sea-level fluctuations on a siliciclastic estuarine shoreline, Delaware Bay, southern New Jersey, USA. Geol. Soc. London, Spec. Publ. 211, 67–77.

Obert, J.C., Scholz, D., Felis, T., Brocas, W.M., Jochum, K.P., Andreae, M.O., 2016. 230Th/U dating of Last Interglacial brain corals from Bonaire (southern Caribbean) using bulk and theca wall material. Geochim. Cosmochim. Acta 178, 20–40. doi:10.1016/j.gca.2016.01.011

Ota, Y., Omura, A., 1991. Late Quaternary Shorelines in the Japanese Islands. Quat. Res. 30, 175–186. doi:10.4116/jaqua.30.175

Otto-Bliesner, B.L., Marshall, S.J., Overpeck, J.T., Miller, G.H., Hu, A., 2006. Simulating Arctic climate warmth and icefield retreat in the last interglaciation. Science (80-.). 311, 1751–1753.

Otvos, E., 2000. Beach ridges—definitions and significance. Geomorphology.

Pavlis, N.K., Holmes, S.A., Kenyon, S.C., Factor, J.K., 2012. The development and evaluation of the Earth Gravitational Model 2008 (EGM2008) Journal of Geophysical Research: Solid Earth (1978-2012) Volume 117, Issue B4

Pedoja, K., Husson, L., Johnson, M.E., Melnick, D., Witt, C., Pochat, S., Nexer, M., Delcaillau, B., Pinegina, T., Poprawski, Y., Authemayou, C., Elliot, M., Regard, V., Garestier, F., 2014. Coastal staircase sequences reflecting sea-level oscillations and tectonic uplift during the Quaternary and Neogene. Earth-Science Rev. 132, 13–38. doi:10.1016/j.earscirev.2014.01.007

Pedoja, K., Husson, L., Regard, V., Cobbold, P.R., Ostanciaux, E., Johnson, M.E., Kershaw, S., Saillard, M., Martinod, J., Furgerot, L., Weill, P., Delcaillau, B., 2011a. Relative sea-level fall since the last interglacial stage: Are coasts uplifting worldwide? Earth-Science Rev. 108, 1–15. doi:10.1016/j.earscirev.2011.05.002

Pedoja, K., Regard, V., Husson, L., Martinod, J., Guillaume, B., Fucks, E., Iglesias, M., Weill, P., 2011b. Uplift of quaternary shorelines in eastern Patagonia: Darwin revisited. Geomorphology 127, 121–142.

Petit, J.R., Jouzel, J., Raynaud, D., Barkov, N.I., Barnola, J.M., Basile, I., Bender, M., Chappellaz, J., Davis, M., Delaygue, G., 1999. Climate and atmospheric history of the past 420,000 years from the Vostok ice core, Antarctica. Nature 399, 429–436.

Pirazzoli, P.A., 1996. Sea-level changes: the last 20 000 years. Wiley Chichester.

Pirazzoli, P.A., 2005. Marine terraces, in: Encyclopedia of Coastal Science. Springer, pp. 632–633.

Pirazzoli, P.A., Radtke, U., Hantoro, W.S., Jouannic, C., Hoang, C.T., Causse, C., Best, M.B., 1991. Quaternary raised coral-reef terraces on Sumba Island, Indonesia. Science (80-.). 252, 1834–1836.

Potter, E.-K., Lambeck, K., 2004. Reconciliation of sea-level observations in the Western North Atlantic during the last glacial cycle. Earth Planet. Sci. Lett. 217, 171–181.

Ramsay, P.J., Cooper, J.A.G., 2001. Late Quaternary Sea-Level Change in South Africa. Quat. Res. 57, 82–90.

Ribolini, A., Aguirre, M., Baneschi, I., Consoloni, I., Fucks, E., Isola, I., Mazzarini, F., Pappalardo, M., Zanchetta, G., Bini, M., 2011. Holocene Beach Ridges and Coastal Evolution in the Cabo Raso Bay (Atlantic Patagonian Coast, Argentina). J. Coast. Res. 276, 973–983.

Rignot, E., Mouginot, J., Morlighem, M., Seroussi, H., Scheuchl, B., 2014. Widespread, rapid grounding line retreat of Pine Island, Thwaites, Smith, and Kohler glaciers, West Antarctica, from 1992 to 2011. Geophys. Res. Lett.

Rovere, A., Antonioli, F., Bianchi, C.N., 2015a. Fixed biological indicators, in: Shennan, I., Long, A.J., Horton, B.P. (Eds.), Handbook of Sea-Level Research. Wiley Online Library, pp. 268–280.

Rovere, A., Casella, E., Vacchi, M., Parravicini, V., Firpo, M., Ferrari, M., Morri, C., Bianchi, C.N., 2014a. Coastal and marine geomorphology between Albenga and Savona(NW Mediterranean Sea, Italy). J. Maps 1–9. doi:10.1080/17445647.2014.933134

Rovere, A., Hearty, P.J., Austermann, J., Mitrovica, J.X., Gale, J., Moucha, R., Forte, A.M., Raymo, M.E., 2015b. Mid-Pliocene shorelines of the US Atlantic Coastal Plain — An improved elevation database with comparison to Earth model predictions. Earth-Science Rev. 145, 117–131. doi:10.1016/j.earscirev.2015.02.007

Rovere, A., Raymo, M.E., O'Leary, M.J., Hearty, P.J., 2012. Crowdsourcing in the Quaternary sea-level community: insights from the Pliocene. Quat. Sci. Rev. 56, 164–166. doi:10.1016/j.quascirev.2012.09.014

Rovere, A., Raymo, M.E., Mitrovica, J.X., Hearty, P.J., O'Leary, M.J., Inglis, J.D., 2014b. The Mid-Pliocene sea-level conundrum: Glacial isostasy, eustasy and dynamic topography. Earth Planet. Sci. Lett. 387, 27–33.

Rovere, A., Vacchi, M., Firpo, M., Carobene, L., 2011. Underwater geomorphology of the rocky coastal tracts between Finale Ligure and Vado Ligure (western Liguria, NW Mediterranean Sea). Quat. Int. 232, 187–200. doi:10.1016/j.quaint.2010.05.016

Rowe, M.P., Wainer, K.A.I., Bristow, C.S., Thomas, A.L., 2014. Anomalous MIS 7 sea-level recorded on Bermuda. Quat. Sci. Rev. 90, 47–59.

Rowley, D.B., Forte, A.M., Moucha, R., Mitrovica, J.X., Simmons, N.A., Grand, S.P., 2013. Dynamic topography change of the eastern United States since 3 million years ago. Science (80-.). 340, 1560–1563.

Rybak, O., Huybrechts, P., 2013. Modeling the configuration of the Greenland ice sheet during the Last Interglacial constrained by ice core data. EGU Gen. Assem. Conf.

Schellmann, G., Beerten, K., Radtke, U., 2008. Electron spin resonance (ESR) dating of Quaternary materials. Quat. Sci. J. 57, 150–178. doi:http://dx.doi.org/10.3285/eg.57.1-2.6

Schellmann, G., Radtke, U., 2000. ESR dating stratigraphically well-constrained marine terraces along the Patagonian Atlantic coast (Argentina). Quat. Int. 68-71, 261–273. doi:10.1016/S1040-6182(00)00049-5

Schellmann, G., Radtke, U., 2004. A revised morpho- and chronostratigraphy of the Late and Middle Pleistocene coral reef terraces on Southern Barbados (West Indies). Earth Sci. Rev. 64, 157–187.

Schellmann, G., Radtke, U., 2010. Timing and magnitude of Holocene sea-level changes along the middle and south Patagonian Atlantic coast derived from beach ridge systems, littoral terraces and valley-mouth terraces. Earth Sci. Rev. 103, 1–30.

Schellmann, G., Radtke, U., Potter, E.K., Esat, T.M., McCulloch, M.T., 2004. Comparison of ESR and TIMS U/Th dating of marine isotope stage (MIS) 5e, 5c, and 5a coral from Barbados—implications for palaeo sea-level changes in the Caribbean. Quat. Int. 120, 41–50.

Schwartz, M., 2005. ENCYCLOPEDIA of COASTAL SCIENCE. Springer.

Schwindt, E., De Francesco, C.G., Iribarne, O.O., 2004. Individual and reef growth of the invasive reef-building polychaete Ficopomatus enigmaticus in a south-western Atlantic coastal lagoon. J. Mar. Biol. Assoc. UK 84, 987–993.

Serrano, D., Ramírez-Félix, E., Valle-Levinson, A., 2013. Tidal hydrodynamics in a two-inlet coastal lagoon in the Gulf of California. Cont. Shelf Res. 63, 1–12.

Seu-Anoï, N.M., Ouattara, A., Koné, Y.J.-M., Gourène, G., 2011. Seasonal distribution of phytoplankton in the Aby lagoon system, Ivory Coast, West Africa. African J. Aquat. Sci. 36, 321–330.

Shennan, I., Horton, B., 2002. Holocene land- and sea-level changes in Great Britain. J. Quat. Sci. 17, 511–526.

Sherman, C.E., Glenn, C.R., Jones, A.T., Burnett, W.C., Schwarcz, H.P., 1993. New evidence for two highstands of the sea during the last interglacial, oxygen isotope substage 5e. Geology 21, 1079–1082.

Short, A. D., 1999. Handbook of beach and shoreface morphodynamics. John Wiley & Sons.

Sivan, D., Gvirtzman, G., Sass, E., 1999. Quaternary stratigraphy and paleogeography of the Galilee coastal plain, Israel. Quat. Res. 51, 280–294.

Spada, G., Stocchi, P., 2007. SELEN: A Fortran 90 program for solving the “sea-level equation.” Comput. Geosci. 33, 538–562.

Stearns, C.E., 1976. Estimates of the position of sea-level between 140,000 and 75,000 years ago. Quat. Res. 6, 445–449.

Stempfhuber, W., Buchholz, M., 2012. a Precise, Low-Cost Rtk Gnss System for Uav Applications. ISPRS - Int. Arch. Photogramm. Remote Sens. Spat. Inf. Sci. XXXVIII-1/, 289–293. doi:10.5194/isprsarchives-XXXVIII-1-C22-289-2011

Stephenson, W.J., 2000. Shore platforms: a neglected coastal feature? Prog. Phys. Geogr. 24, 311–327.

Stephenson, W.J., Kirk, R.M., 2000. Development of shore platforms on Kaikoura Peninsula, South Island, New Zealand: II: The role of subaerial weathering. Geomorphology 32, 43–56.

Stirling, C.H., Andersen, M.B., 2009. Uranium-series dating of fossil coral reefs: Extending the sea-level record beyond the last glacial cycle. Earth Planet. Sci. Lett. 284, 269–283.

Stirling, Esat, Lambeck, McCulloch, 1998. Timing and duration of the Last Interglacial: evidence for a restricted interval of widespread coral reef growth. Earth Planet. Sci. Lett. 160, 18.

Storlazzi, C.D., Logan, J.B., Field, M.E., 2003. Quantitative morphology of a fringing reef tract from high-resolution laser bathymetry: Southern Molokai, Hawaii. Geol. Soc. Am. Bull. 115, 1344.

Suga, N., Montani, S., 2012. The Effect of Microphytobenthic Resuspension on Suspended Particulate Matter Dynamics in a Shallow Lagoon in Hokkaido, Japan. Interdiscip. Stud. Environ. Chem. Environ. Pollut. Ecotoxicol. 353–365.

Sunamura, T., 1992. Geomorphology of rocky coasts. John Wiley & Son Ltd.

Surić, M., Lončarić, R., Lončar, N. 2009. Submerged caves of Croatia: distribution, classification and origin. Environmental Earth Sciences, 1-8.

Surić, M., Richards, D.A., Hoffmann, D.L., Tibljas, D., Juracic, M. 2009. Sea-level change during MIS 5a based on submerged speleothems from the eastern Adriatic Sea (Croatia). Marine Geology, 262, 62-67.

Takasu, T., Yasuda, A., 2009. Development of the low-cost RTK-GPS receiver with an open source program package RTKLIB. Int. Symp. GPS/GNSS.

Tamura, T., 2012. Beach ridges and prograded beach deposits as palaeoenvironment records. Earth-Science Rev. 114, 279–297. doi:10.1016/j.earscirev.2012.06.004

Ten Hove, H.A., 1979. Different causes of mass occurrence in serpulids. Biol. Syst. Colon. Org. 11, 281–298.

Ten Hove, H.A., Weerdenburg, J.C.A., 1978. A generic revision of the brackish-water serpulid Ficopomatus Southern 1921 (Polychaeta: Serpulinae), including Mercierella Fauvel 1923, Sphaeropomatus Treadwell 1934, Mercierellopsis Rioja 1945 and Neopomatus Pillai 1960. Biol. Bull. 154, 96–120.

Thompson, W.G., Curran, H.A., Wilson, M.A., White, B., 2011. Sea-level oscillations during the last interglacial highstand recorded by Bahamas corals. Nat. Geosci. 4, 684–687.

Tintoré, J., Medina, R., Gómez-Pujol, L., Orfila, A., Vizoso, G., 2009. Integrated and interdeisciplinary scientific approach to coastal management. Ocean Coast Manage. 52, 493-505.

Tintoré et al., 2013. SOCIB: The Balearic Islands Coastal Ocean Observing and Forecasting System. Responding to Science, Technology and Society Needs. Marine Technology Society Journal, 47: 101-117.

Tormey, B.R., 2007. Rapid Sea-Level Change And Intensified Storms During The Last Interglacial: A High Resolution Record From The Bahamas, in: 2007 GSA Denver Annual Meeting.

Trenhaile, A.S., 1987. The geomorphology of rock coasts. Oxford University Press, USA.

Trenhaile, A.S., 2008. Modeling the role of weathering in shore platform development. Geomorphology 94, 24–39.

Trenhaile, A.S., Kanyaya, J.I., 2007. The Role of Wave Erosion on Sloping and Horizontal Shore Platforms in Macro- and Mesotidal Environments. J. Coast. Res. 232, 298–309.

Trenhaile, A.S., Porter, N.J., 2007. Can shore platforms be produced solely by weathering processes? Mar. Geol. 241, 79–92.

Trowbridge, A.C., 1954. Mississippi River and Gulf Coast terraces and sediments as related to Pleistocene history—a problem. Geol. Soc. Am. Bull. 65, 793–812.

Tulipani, S., Grice, K., Krull, E., Greenwood, P., Revill, A.T., 2014. Salinity variations in the northern Coorong Lagoon, South Australia: Significant changes in the ecosystem following human alteration to the natural water regime. Org. Geochem. 75, 74–86.

Turney, C.S.M., Jones, R.T., 2010. Does the Agulhas Current amplify global temperatures during super-interglacials? J. Quat. Sci. 25, 839–843.

US Army Corps Of Engineers, 1984. "Shore protection manual." *Army Engineer Waterways Experiment Station, Vicksburg, MS. 2v* (1984): 37-53.

Vacchi, M., Montefalcone, M., Schiaffino, C.F., Parravicini, V., Bianchi, C.N., Morri, C., Ferrari, M., 2014. Towards a predictive model to assess the natural position of the Posidonia oceanica seagrass meadows upper limit. Mar. Pollut. Bullettin 83, 458–66. doi:10.1016/j.marpolbul.2013.09.038

Vacchi, M., Rovere, A., Zouros, N., Desruelles, S., Caron, V., Firpo, M., 2012. Spatial distribution of sea-level markers on Lesvos Island (NE Aegean Sea): Evidence of differential relative sea-level changes and the neotectonic implications. Geomorphology 159-160, 50–62.

Vacchi, M., Marriner, N., Morhange, C., Spada, G., Fontana, A., Rovere, A., 2016. Multiproxy assessment of Holocene relative sea-level changes in the western Mediterranean: variability in the sea-level histories and redefinition of the isostatic signal. Earth Sci. Rev. 155, 172-197.

Vesica, P., Tuccimei, P., Turi, B., 2000. Late Pleistocene Paleoclimates and sea-level change in the Mediterranean as inferred from stable isotope and U-series studies of overgrowths on speleothems, Mallorca, Spain. Quat. Sci. Rev. 19, 1–15.

Vesica, P.L., Tuccimei, P., Turi, B., Fornós, J.J., Ginés, A., Ginés, J., 2000. Late Pleistocene Paleoclimates and sea-level change in the Mediterranean as inferred from stable isotope and U-series studies of overgrowths on speleothems, Mallorca, Spain. Quaternary Science Reviews, 19, 865-879.

Wehmiller, J.F., 2013. United States Quaternary coastal sequences and molluscan racemization geochronology--what have they meant for each other over the past 45 years? Quat. Geochronol. 16, 3–20.

Woodroffe, C.D., McGregor, H. V, Lambeck, K., Smithers, S.G., Fink, D., 2012. Mid-Pacific microatolls record sea-level stability over the past 5000 yr. Geology 40, 951–954.

Woodroffe, C.D., Murray-Wallace, C.V., Bryant, E.A., Brooke, B., Heijnis, H., Price, D.M., 1995. Late Quaternary sea-level highstands in the Tasman Sea: evidence from Lord Howe Island. Mar. Geol. 125, 61–72. doi:10.1016/0025-3227(95)00028-W

Zazo, C., Goy, J.L., Dabrio, C.J., Bardají, T., Hillaire-Marcel, C., Ghaleb, B., González-Delgado, J.-Á., Soler, V., 2003. Pleistocene raised marine terraces of the Spanish Mediterranean and Atlantic coasts: records of coastal uplift, sea-level highstands and climate changes. Mar. Geol. 194, 103–133.

Zazo, C., Goy, J.L., Dabrio, C.J., Soler, V., Hillaire-Marcel, C., Ghaleb, B., González-Delgado, J.A., Bardají, T., Cabero, A., 2007. Quaternary marine terraces on Sal Island (Cape Verde archipelago). Quat. Sci. Rev. 26, 876–893.

Zazo, C., Silva, P.G., Goy, J.L., Hillaire-Marcel, C., Ghaleb, B., Lario, J., Bardají, T., González, A., 1999. Coastal uplift in continental collision plate boundaries: Data from the Last Interglacial marine terraces of the Gibraltar Strait area (south Spain). Tectonophysics 301, 95–109. doi:10.1016/S0040-1951(98)00217-0

Zecchin, M., Nalin, R., Roda, C., 2004. Raised Pleistocene marine terraces of the Crotone peninsula (Calabria, southern Italy): facies analysis and organization of their deposits. Sediment. Geol. 172, 165–185.

FIGURE CAPTIONS

Figure 1 Example of calculation of RWL, IR, RSL and RSL error from a paleo RSL indicator (marine terrace) and a modern analog.

Figure 2 Difference between RSL, terrestrial and marine limiting points. The Pleistocene dune of Cerveteri is described in Nisi et al., 2003 and references therein. The deposits at Grot Brak are described in Carr et al., 2010. The Plio-Pleistocene marine facies in Pianosa Island are described in Graciotti et al., 2002.

Figure 3 Number of a) sites and b) papers published within land parcels of 500 square kilometers; c) number of studies reporting MIS 5e shorlines per year; d) error bars on MIS 5e sea-level. Based on data from Pedoja et al., 2014.

Figure 4. Landforms commonly used as RSL indicators for MIS 5e with the upper and lower limits of the Indicative Range shown by the thin dark blue lines (see Table 3 for more details and definitions).

Figure 5 a) Example of an MIS 5e marine terrace on Santa María Island, Azores (see Avila et al., 2015 for details); b) modern inner margin of marine terrace located in the swash zone, being actively shaped by beach erosion processes (Portugal, Algarve); c) modern inner margin located near the breaking depth of waves at around 4-5m depth (NW Italy, Capo Noli, Rovere et al., 2014a, 2011). The gray line in each figure represents the location of the inner margin.

Figure 6 a) Reef flat in Malé Atoll, Maldives; b) frequency distribution of the maximum reef flat depth of 34 reefs worldwide (see supplementary materials for details); c) the location of these reefs. References: 1. Falter et al., 2013; 2. Jokiel et al., 2014; 3. Storlazzi et al., 2003; 4. Mariath et al., 2013; 5. Lasagna et al., 2010; 6. Buddemeier et al., 1975; 7. Kench and Brander, 2006; 8. Goatley and Bellwood, 2012; 9. Dean et al., 2015; 10. Mongin and Baird, 2014; Other datasets: Blanchon, 2011; Montaggioni, 2005.

Figure 7 Modern shore platforms in a) South Africa, De Hoop Nature Reserve and b) Guadeloupe, French Caribbean; c) modern shore platform in Galilee, Israel. The green line separates the modern platform from an upper platform shaped during MIS 5e (Sivan et al., 1999); d) MIS 5e shore platform (green line) on Santa Maria Island, Azores ("Pedra que Pica" outcrop, for details see Avila et al., 2015); e) deposits still preserved on the Santa Maria platform include rounded boulders of volcanic origin with fossil limpets (*Patella* sp.) still attached in living position. Such observations can be used to better constrain the indicative range of this deposit as the preferred habitat of *Patella* is generally ranges between the supra-littoral zone and the spray zone (Rovere et al., 2015a); f) Potholes (green arrows) on a shore platform in Biddiriscottai, Sardinia, NW Italy, that are shaped during winter storms.

Figure 8 a) Last Interglacial beach deposit in Grape Bay, Bermuda (Hearty, 2002; Hearty et al., 1992). The observed sedimentary structures suggest a sequence where water depth? is shoaling upwards. The paleo RSL is best placed at the top of the foreshore beds; b) last interglacial beach deposit in Campo de Tiro, Mallorca, Spain (Hearty, 1987) where no diagnostic sedimentary structures have been preserved. In c) a detail of the same deposit shows that it contains fragments of shells and small pebbles. The indicative range of this deposit cannot be constrained to better than the general range shown in Figure 4d; d) contact (white line) between planar laminations and beach berm horizons on a modern beach near Keta, Ghana.

Figure 9 Late Holocene beachrock in a) Liguria, NW Italy (Rovere et al., 2014a); and b) Maui, Hookipa Park, Hawaii (Meyers, 1987).

Figure 10 a) Back of a Last Interglacial beach ridge in Camarones, Argentina, cut by roadworks (see Fig. 6 in Schellmann and Radtke, 2000); b) detail of the same beach ridge, showing a layer of pebbles and imbricated shells near the top of the ridge.

Figure 11 a) Coastal lagoon near Jandia, Fuerteventura, Spain. The maximum depth of the lagoon is -1.5m. It is separated from the open ocean by a sand bar; b) frequency distribution of the maximum depth of lagoons worldwide based on 42 locations (see supplementary materials for details); c) the location of these lagoons. References: 1. Hanna et al., 2014; 2. Serrano et al., 2013 ; 3. Nicholls, 1989; 4. Contreras et al., 2014; 5. De Francesco and Isla, 2003; 6. Bruneau et al., 2011; 7. Dias et al., 2001; 8. Bellucci et al., 2002 ; 9. Bonnet et al., 2012; 10. Karroubi et al., 2012; 11. Lamptey et al., 2013; 12. Seu-Anoi et al., 2011; 13. Chandana et al., 2008; 14. Nagasaka and Takano, 2014; 15. Suga and Montani, 2011; 16. Tulipani et al., 2014.

Figure 12 a) Modern chenier ridge at the estuary of the Volta River, Ghana; b) aerial view with indication of the location where the photo in a) has been taken. The maximum elevation of this chenier above sea-level is 2.3m.

Figure 13 Modern tidal notches in a) Krabi, Thailand, and b) Cottesloe Beach, Perth, Western Australia; Last Interglacial tidal notches in c) Capo S. Vito, Sicily; and d) and e) preserved on vertical cliffs in the Orosei Gulf, Sardinia, Italy (Antonioli et al., 2006; Carobene, 2014). The notch is indicated by the black dashed line; f) a tidal notch in Biddiriscottai, Dorgali, Sardinia, partially covered by aeolianites of last glacial maximum age (Antonioli et al., 2015).

Figure 14 a), b) Abrasion notches at Capo Noli, Italy, NW Mediterranean Sea. The length of the stick is 1.5 m; c) abrasion notch formed inside a coastal cave, Cap D'Agde, southern France; d) ??and ??e) perspective photo and scheme of a coastal cave formed by abrasion in highly fractured conglomerates in Portofino, NW Italy. The cave formed along a major fault in the bedrock and is still actively being modified by abrasion. The abrasion occurs by pebbles mobilized by wave action. The cave is few meters wide and deepens with a trapeziodal shape. Perspective photo in d) by Regione Liguria.

Figure 15 a) Cala Millor, on the Island of Mallorca, Spain. The bathymetry and topography are derived from single beam and GPS surveys (10/07/2012). The gray transect line shows the location of Figure 15e and the white rectangle shows the area where Unmanned Aerial Vehicle (UAV) surveys were performed, as detailed in c); b) the site where the MIS 5e beach deposit outcrops with measurements of the upper and lower elevations of the outcrop; c) Orthophoto and digital elevation model obtained from UAV surveys and structure from motion techniques (Casella et al., 2014, 2016). The beach berm has been identified in the DEM at an average elevation of +0.8m (see also histograms in e); d) data obtained from a pressure sensor located at -1.6m depth in the study area, from which we calculate significant wave height in 15 minutes bins (Hs, lower x axis) and the relative frequency of wave heights (upper x axis, dashed line); e) right side: histograms and gaussian showing the depth of the longshore bar derived from bathymetric data in a) and the elevation of the maximum wave runup (proxy for the beach berm) derived from topographic data in c,d); center: topography of the beach, with measured elevations and position of RWL and IR; left: Age/elevation plot showing position of calculated paleo RSL, compared with that obrained in a nearby cave by Vesica et al. (2000).

Figure 16 a) and b) sea-level scenarios for MIS 5e obtained from ANICE, a global ice-sheet model (de Boer et al., 2014). c) and d) show the GIA predictions calculated in Cala Millor, Mallorca, for each of the two sea-level scenarios. The predictions obtained using three mantle viscosities are shown in different line colors (see box: UM=Upper Mantle, TZ=Transition Zone, LM=Lower Mantle); e) sea-level scenarios used in this study (dashed lines) compared with the Last Interglacial sea-level history obtained by Kopp et al., 2009. The solid gray line indicates the median projection of Kopp et al., the light gray bands the 16^{th} and 84^{th} percentiles and the dark grey band the 2.5^{th} and 97.5^{th} percentiles (redrawn from Kopp et al., 2009); f) relative frequency of long-term rates of post-depositional displacement calculated in time steps of 1 ka using data in panels a-d and a paleo RSL of 1.8±1.4 m.

*Abstract

Abstract

The Last Interglacial (MIS 5e, 128-116 ka) is among the most studied past periods in Earth's history. The climate at that time was warmer than today, primarily due to different orbital conditions, with smaller ice sheets and higher sea-level. Field evidence for MIS 5e sea-level was reported from thousands of sites, but often paleo shorelines were measured with low-accuracy techniques and, in some cases, there are contrasting interpretations about paleo sea-level reconstructions. For this reason, large uncertainties still surround both the maximum sea-level attained as well as the pattern of sea-level change throughout MIS 5e. Such uncertainties are exacerbated by the lack of a uniform approach to measuring and interpreting the geological evidence of paleo sea-levels. In this review, we discuss the characteristicsof MIS 5e field observations, and we set the basis for a standardized approach to MIS 5e paleo sea-level reconstructions, that is already successfully applied in Holocene sea-level research. Application of the standard definitions and methodologies described in this paper will enhance our ability to compare data from different research groups and different areas, in order to gain deeper insights into MIS 5e sea-level changes. Improving estimates of Last Interglacial sea-level is, in turn, a key to understand the behavior of ice sheets in a warmer world.

Table1

Table 1. Relevant equations in MIS 5e paleo sea level studies, with definitions. For a calculator containing the equations in this table, see the spreadsheet in the supplementary material.

	Equation	Definitions
Eq.1	$RWL = \left[\frac{(U_l + L_l)}{2}\right]$	**RWL=**Reference Water Level **IR**= Indicative Range $\mathbf{U_l}$ = Upper limit of landform in the modern analog $\mathbf{L_l}$ = Lower limit of landform in the modern analog **RSL=**paleo Relative Sea Level **E=** elevation od sea-level indicator(measured in the field) $\mathbf{E_e}$=Error in elevation measurement (standard deviation) $\boldsymbol{\delta_{RSL}}$= uncertainty of RSL (standard deviation) **PD =** Post-depositional displacement uplift / subsidence **PDr=** Post-depositional displacement uplift / subsidence rate $\boldsymbol{\delta_{PDr}}$= uncertainty of PDr (standard deviation) **GIA** = Glacio-hydro-isostatic Adjustment contribution **ESL** = Paleo Eustatic Sea Level **T =** age of the paleo RSL indicator $\boldsymbol{\delta_{GIA}}$= uncertainty of GIA (standard deviation) $\boldsymbol{\delta_{ESL}}$= uncertainty of ESL (standard deviation) $\boldsymbol{\delta_T}$ = uncertainty of T (standard deviation)
Eq.2	$IR = (U_l - L_l)$	
Eq.3	$RSL = (E - RWL)$	
Eq.4	$\delta_{RSL} = \sqrt{E_e^2 + \left(\frac{IR}{2}\right)^2}$	
Eq.5a	$PD = [RSL - (GIA + ESL)]$	
Eq.5b	$ESL = [RSL - (GIA + PD)]$	
Eq.6	$PDr = \left[\frac{RSL - (GIA + ESL)}{T}\right]$	
Eq.7a	$\delta_{PD} = \sqrt{(\delta_{RSL}^2 + \delta_{GIA}^2 + \delta_{ESL}^2)}$	
Eq.7b	$\delta_{ESL} = \sqrt{(\delta_{RSL}^2 + \delta_{GIA}^2 + \delta_{PD}^2)}$	
Eq.8	$\delta_{PDr} = \sqrt{\left(\frac{\delta_{PD}^2}{T^2}\right) + \left[\left(\frac{PD}{T^2}\right)^2 \times \delta T^2\right]}$	

Table2

Table 1. Description of the vertical accuracy and error of techniques used to measure elevations in the field.

Measurement technique	Description	Typical vertical error under optimal conditions
Differential GPS	Positions are acquired in the field and are corrected, either in real time or during post-processing, with respect to the known position of a base station or a geostationary satellite system (e.g. Omnistar). Accuracy depends on satellite signal strength, distance from base station, and number of static positions acquired at the same location.	±0.02 / ±0.08 m
Total station	Total stations or levels measure slope distances from the instrument to a particular point and triangulate relative to the XYZ coordinates of the base station. The accuracy of this process depends on how well defined the reference point and on the distance of the surveyed point from the base station. Thus, it is necessary to benchmark the reference station with a nearby tidal datum, or use a precisely (DGPS) known geodetic point. the accuracy of the elevation measurement is also inversely proportional to the distance between the instrument and the point being measured.	±0.1 / ±0.2 m
Auto or hand level		±0.2 / ±0.4 m
Metered tape or rod	The end of a tape or rod is placed at a known coordinate or elevation point, and the elevation of the unknown point is calculated using the metered scale and, if necessary, clinometers to calculate angles. The accuracy of this method decreases considerably with elevation offsets greater than 10 meters between the known and unknown points.	Up to ±10% of elevation measurement
Barometric altimeter	Difference in barometric pressure between a point of known elevation (often sea level) and a point of unknown elevation. Not accurate and used only rarely (e.g. Pedoja et al., 2011b)	Up to ±20% of elevation measurement
Topographic map and digital elevation models	Elevation derived from the contour lines on topographic maps. Most often used for large-scale landforms (i.e. marine terraces). Several meters of error are possible, depending on the scale of the map or the resolution of the DEM (Rovere et al., 2015b).	Variable with scale of map and technique used to derive DEM.

Table3

Table 1 Summary of landforms most commonly used in last interglacial sea level studies, including upper and lower limits of indicative range as described in the text and elements within the landform that might help inform the indicative range. In the last column, each parameter used in the table and in the text is described.

Landform	Upper limit	Lower limit	Elements improving RSL estimate	Definitions
Marine terraces	Storm wave swash height (SWSH)	Breaking depth (d_b)	Presence of fixed biological indicators or sedimentary features in the deposits covering the terrace.	**MHHW**: mean higher high water, the average of the higher high water height of each tidal day observed over a Tidal Datum Epoch (NOAA). **MLLW**: mean lower low water, the average of the lower low water height of each tidal day observed over a Tidal Datum Epoch (NOAA). **SWSH**: storm wave swash height, it is the maximum elevation reached by extreme storms on the beach (Otvos, 2000). ***d_b***: breaking depth. Horizontal water particle velocities reach their maximum values at the breaking depth, so that the sea floor beneath the breaker zone is where the coarsest sediments are trained or brought into suspension. This zone is function of the wave climate and can be empirically calculated knowing average annual wave period and wave height, wave approach angle, and coefficients depending on the slope and type of coast. In absence of site-dependent data, db can be calculated using the dimensionless parameter H/d. This parameter is used for the relative height of the wave compared to the water depth, and is often used to determine wave breaking criteria. For a smooth, flat slope, the maximum ratio of $H/d_b = 0.78$ (therefore $d_b=H/0.78$) is commonly used for wave breaking criteria, and increases as the bottom slope increases (U.S. Army Corps of Engineers, 1984). **EFR**: end of forereef, the break in slope marking the transition between the quasi-horizontal surface shaped by waves and the reef slope. **ob**: ordinary berm. Berms are depositional features formed by the wave-induced accumulation of sand on the beach (Schwartz, 2005). The ordinary berm is the one produced by average or more typical waves. The elevation of the berm depends on wave climate and sediment size, and it can be assumed that it is function of ordinary wave runup. The berm can be either measured at the modern analog or deduced from the wave runup calculated using models. In absence of site-dependent data, to estimate runup once can adopt the empirical formula $R/Hs= \alpha$ (Mayer and Kriebel, 1994) where R is the wave runup and α depends on wave properties and beach slope. Usually, α is estimated empirically between $0.1<\alpha<0.3$ for regular waves acting on uniform, smooth, and impermeable laboratory beaches with slopes typical of many natural beach slopes. Once can ideally set α as the average of the two values, i.e. 0.2, and add to R the value of MHHW, as an high tide would be responsible for shifting upwards the runup height. Therefore $ob=R+MHHW=(Hs*0.2)+MHHW$. **sz**: spray zone, above the MHHW and regularly splashed but not submerged by ocean water. It is very difficult to define the elevation range of the spray zone without observations of a modern analog. As an approximation, one can adopt as a sz value twice the elevation of the ordinary berm calculated as described above. **ld**: the depth of the lagoon bottom, usually very shallow. **ec**: elevation of chenier, up to few meters above sea level.
Coral reef terraces	Mean lower low water (MLLW)	End of forereef (EFR)	Living ranges of different species, or particular growth forms (e.g. microatolls).	
Shore platforms	Mean higher high water (MHHW)	Between Mean Lower Low Water and breaking depth (d_b +MLLW)/2	Presence of biological indicators.	
Beach deposits	Ordinary berm (ob)	Breaking depth (d_b)	Biofacies, orientation and integrity of shells, sedimentary structures.	
Beachrock	Spray zone (sz)	Breaking depth (d_b)	Sedimentary structures, types of cement.	
Beach ridges	Storm wave swash height (SWSH)	Ordinary berm (ob)	Sedimentary structures	
Lagoon deposits	Mean lower low water (MLLW)	Depth of lagoon bottom (ld)	Sedimentary structures, presence of biological indicators or species with limited depth ranges or upper limits in their depth range (i.e. MLLW).	
Cheniers	Elevation of chenier above sea level (ec)	Mean higher high water (MHHW)	Biological indicators or sedimentary structures.	
Tidal notches	Mean higher high water (MHHW)	Mean lower low water (MLLW)	Fixed biological indicators	
Abrasion notches and sea caves	Storm wave swash height (SWSH)	Breaking depth (d_b)	Fixed biological indicators, despite difficult to find due to abrasion.	

Table4

Table 1 Most common dating methods used in Last Interglacial studies.

Method	Typical uncertainty in ka (1-sigma)	Examples
Absolute dating methods		
U-Series	0.5-4 ka	Stirling and Andersen, 2009; Dutton and Lambeck, 2012; Obert et al., 2016.
Optically stimulated luminescence	3-7 ka	Mauz et al., 2015; Carr et al., 2010.
Electro spin resonance	14-20 ka	Pirazzoli et al., 1991; Schellmann et al., 2008.
Thermo luminescence	15-20 ka or limiting ages (e.g. deposit older than 60 ka)	Woodroffe et al., 1995, Mauz and Hassler, 2000.
Relative dating methods		
Amino acid racemization	Usually relative dating methods help to discern between different interglacials.	Hearty and Kaufman, 2000; Wehmiller, 2013.
Biostratigraphy		Avila et al., 2015
Chronostratigraphic correlation		Choi et al., 2008

Figure1

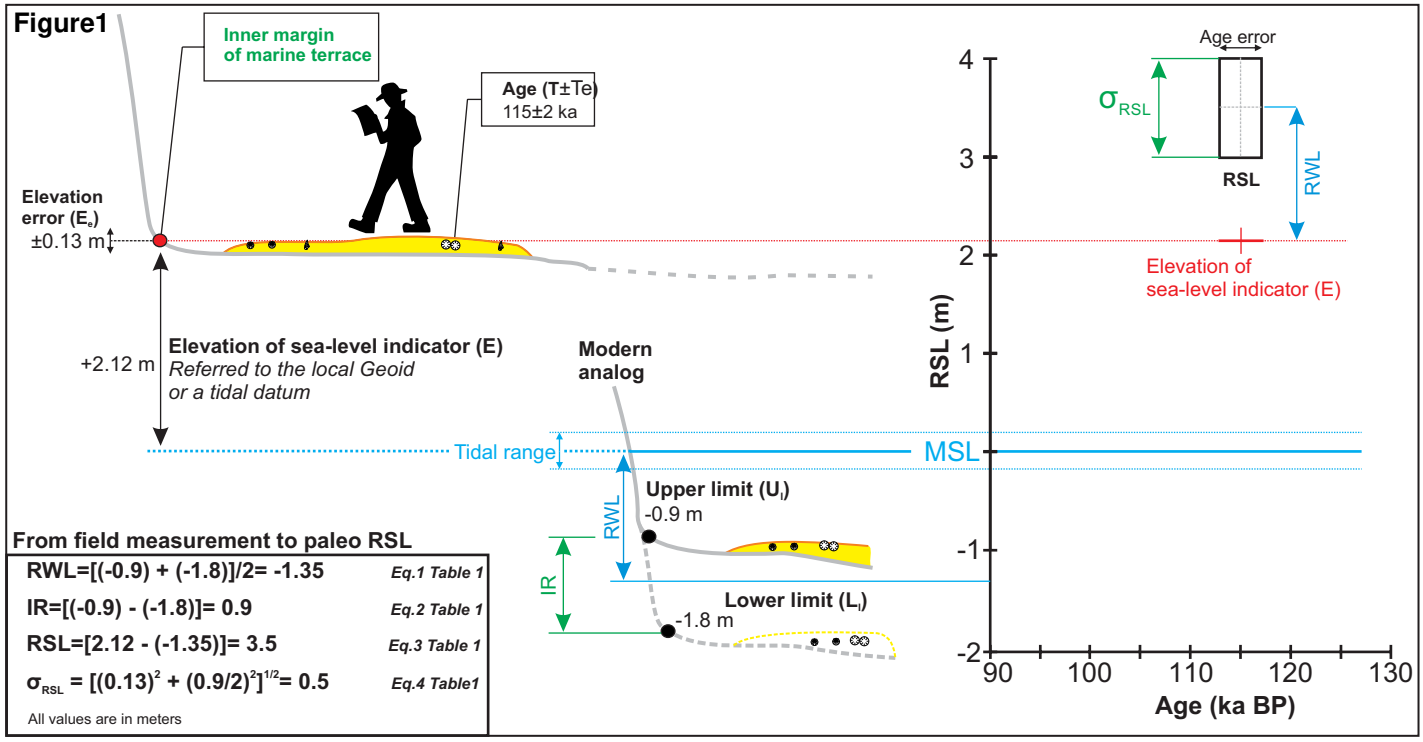

From field measurement to paleo RSL

RWL=[(-0.9) + (-1.8)]/2= -1.35	***Eq.1 Table 1***
IR=[(-0.9) - (-1.8)]= 0.9	***Eq.2 Table 1***
RSL=[2.12 - (-1.35)]= 3.5	***Eq.3 Table 1***
$\sigma_{RSL} = [(0.13)^2 + (0.9/2)^2]^{1/2} = 0.5$	***Eq.4 Table1***

All values are in meters

Figure2

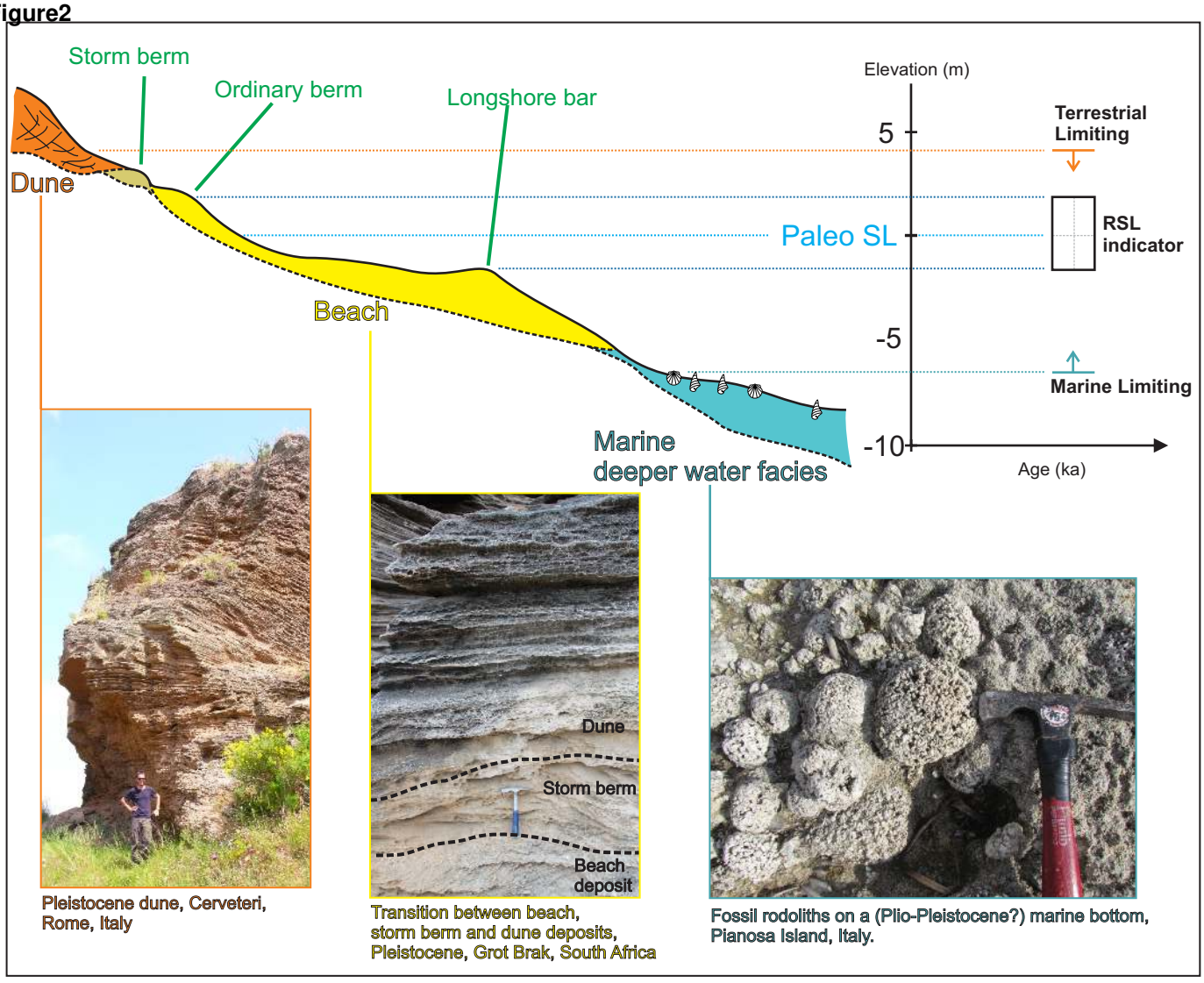

Pleistocene dune, Cerveteri, Rome, Italy

Transition between beach, storm berm and dune deposits, Pleistocene, Grot Brak, South Africa

Fossil rodoliths on a (Plio-Pleistocene?) marine bottom, Pianosa Island, Italy.

Figure3

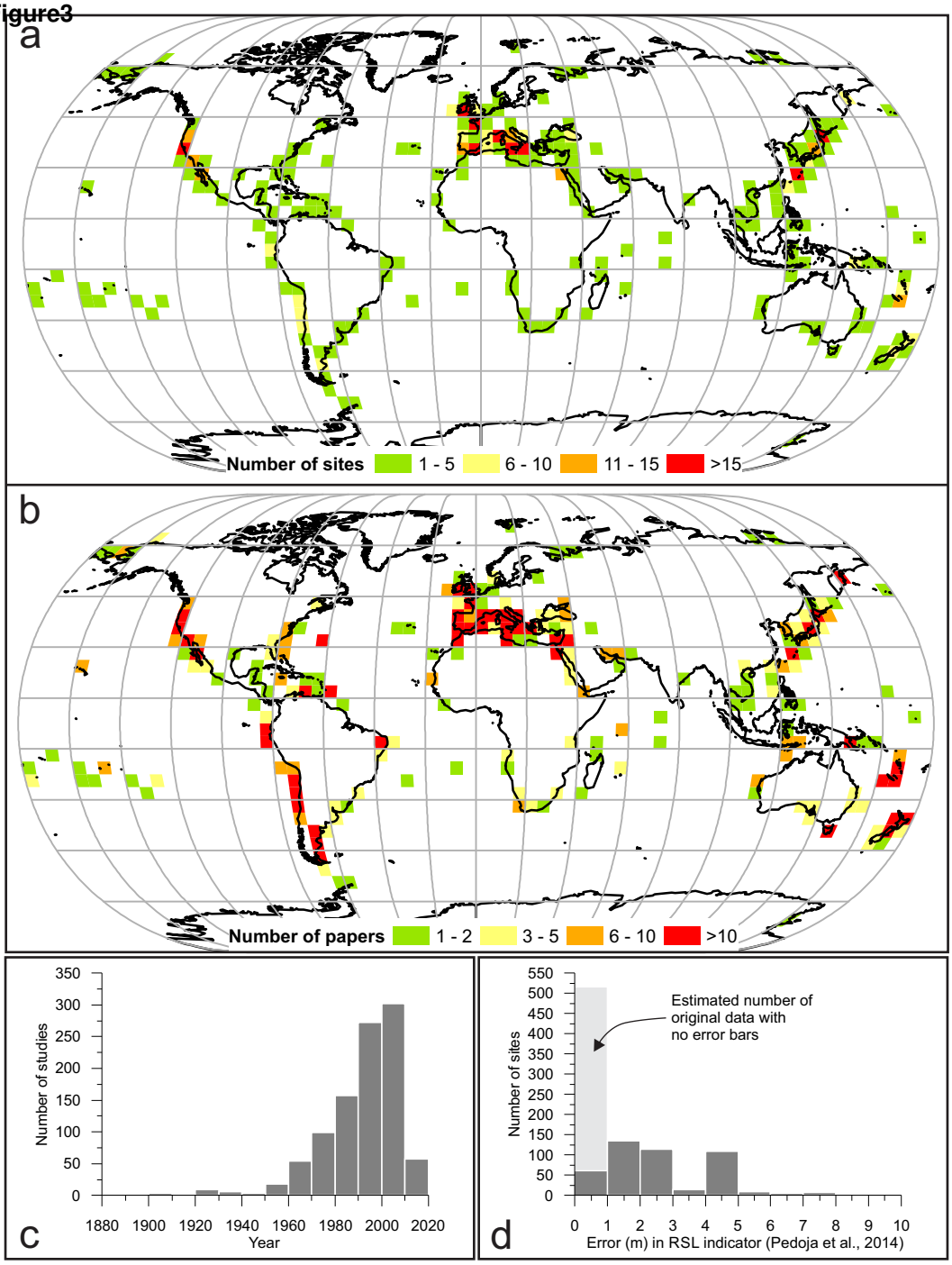
a
Number of sites
1 - 5
6 - 10
11 - 15
>15
b
Number of papers
1 - 2
3 - 5
6 - 10
>10
c
Number of studies
350
300
250
200
150
100
50
0
1880
1900
1920
1940
1960
1980
2000
2020
Year
d
Number of sites
550
500
450
400
350
300
250
200
150
100
50
0
Estimated number of
original data with
no error bars
0
1
2
3
4
5
6
7
8
9
10
Error (m) in RSL indicator (Pedoja et al., 2014)

Figure4

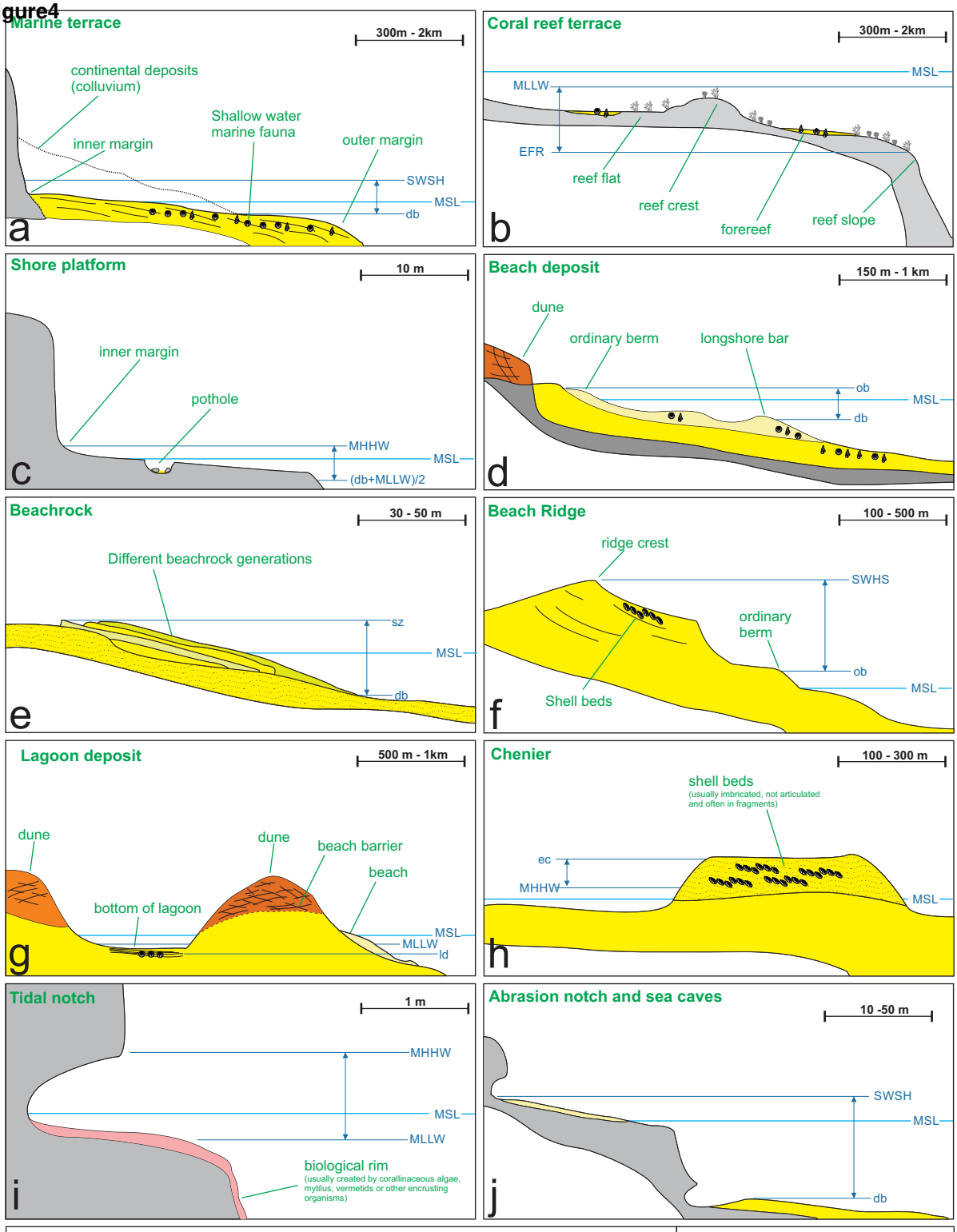

MSL - Mean Sea Level
MHHW - Mean Higher High Water
MLLW - Mean Lower Low Water
EFR - End of forereef
ec - elevation of chenier above sea level

db - Breaking depth
ob - Ordinary berm
sz - Spray zone
SWSH - Storm Wave Swash Height
ld - Depth of lagoon bottom

Rock/cliff
Beach/marine sands
Aeolian sands
Marine fauna (mollusks, corals)

Figure5

Figure6


a

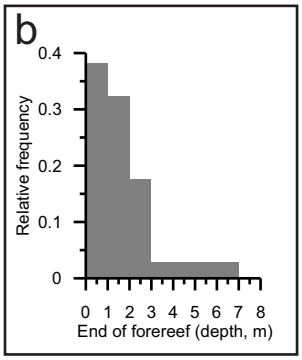
b
0.4
0.3
0.2
0.1
0
Relative frequency
0 1 2 3 4 5 6 7 8
End of forereef (depth, m)

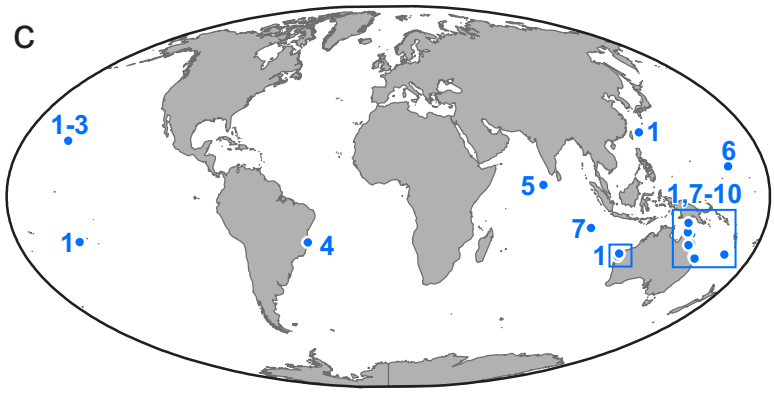
c
1-3
1
4
1
5
7
1
6
1,7-10

Figure7

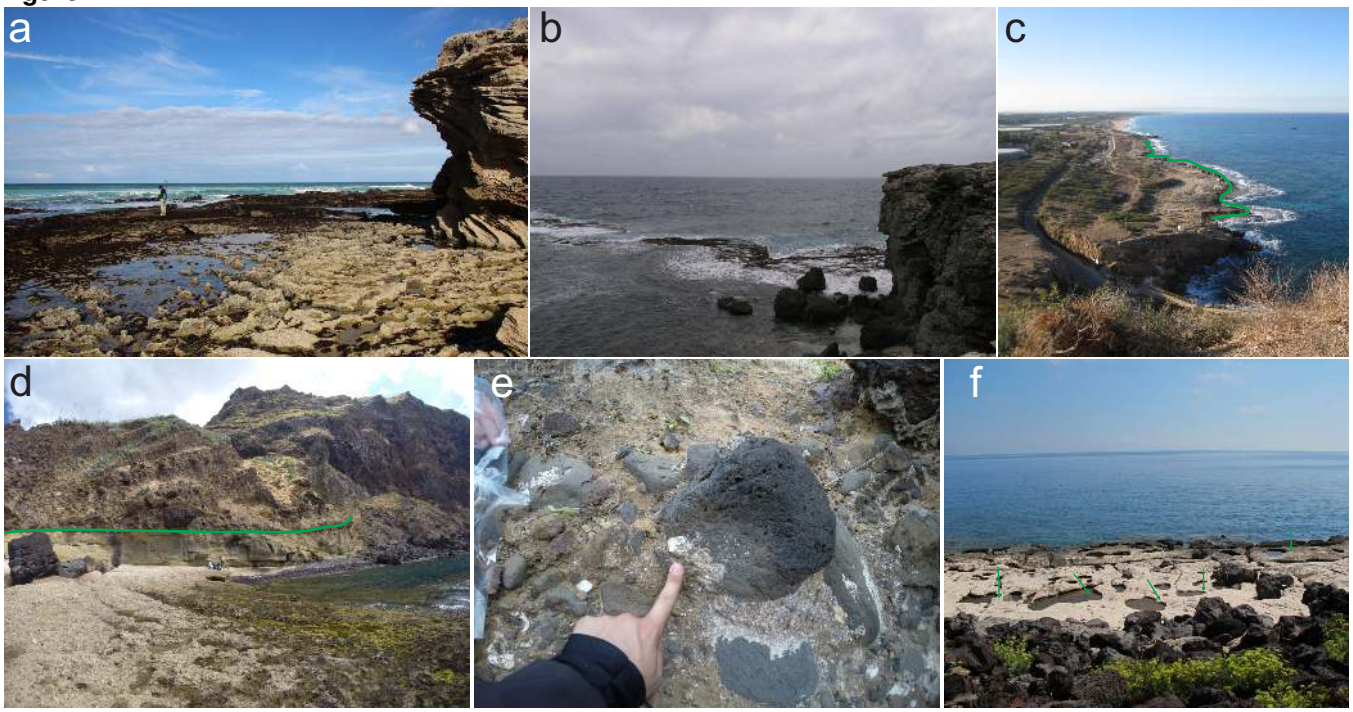

Figure8


a
Planar lamination
(foreshore)
Cross-bedding
(upper shoreface)
Ripple beds
(subtidal)
b
Beach
deposit
30 cm
c
5 cm
d
Beach berm
Upper foreshore
80 cm

Figure9

Figure10

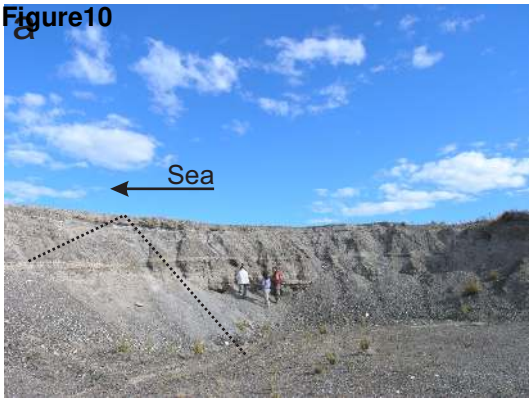

Figure11

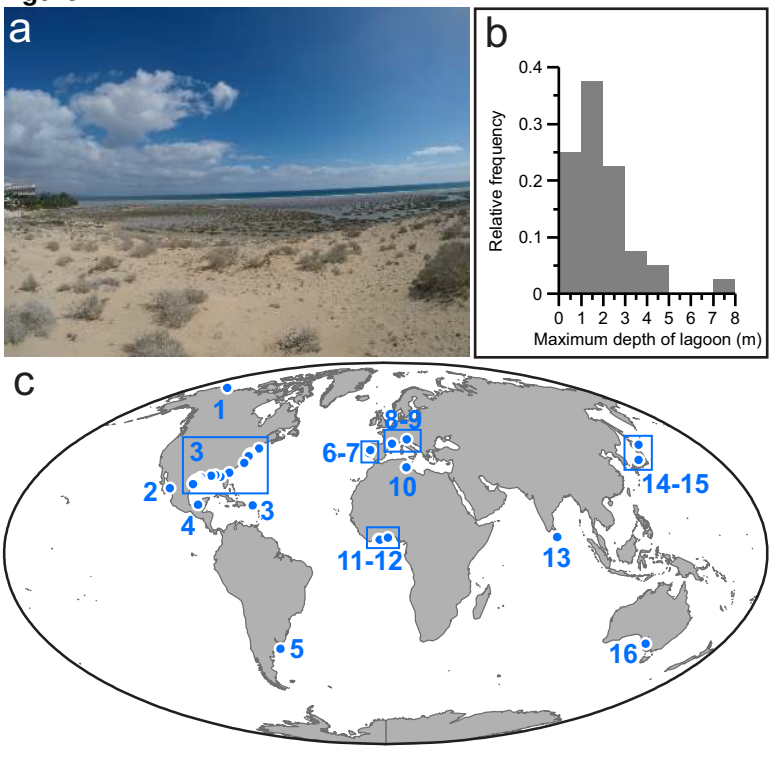
a
b
Relative frequency
0.4
0.3
0.2
0.1
0
0 1 2 3 4 5 6 7 8
Maximum depth of lagoon (m)
c
1
2
3
4
5
6-7
8-9
10
11-12
13
14-15
16

Figure12

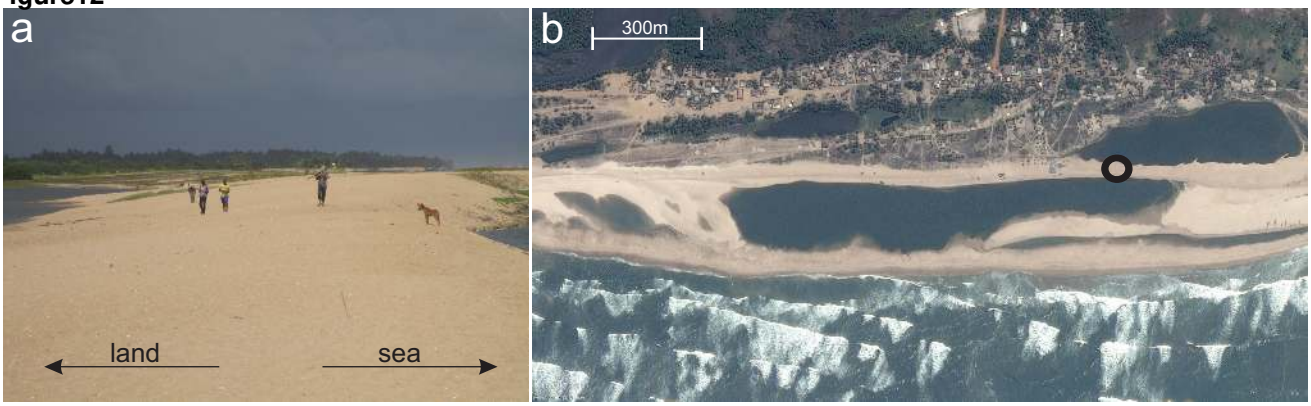

Figure13

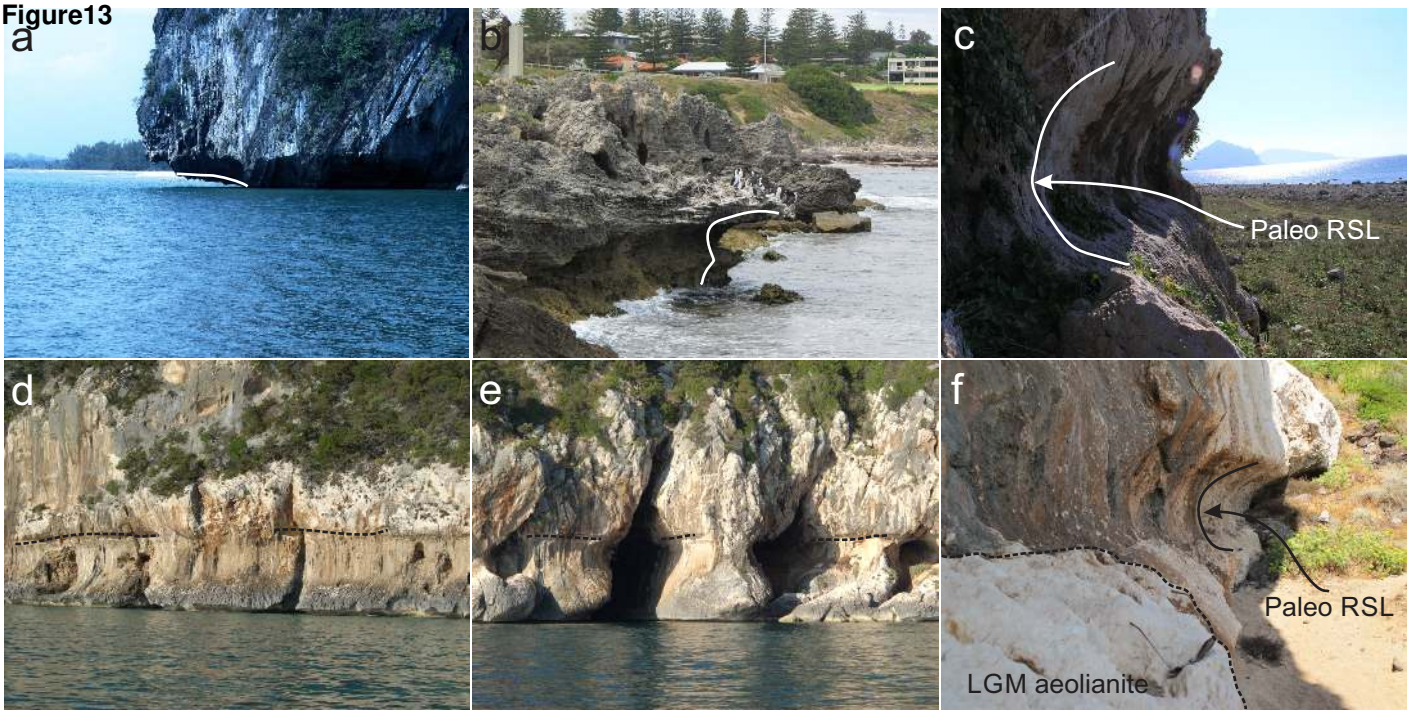

Figure14

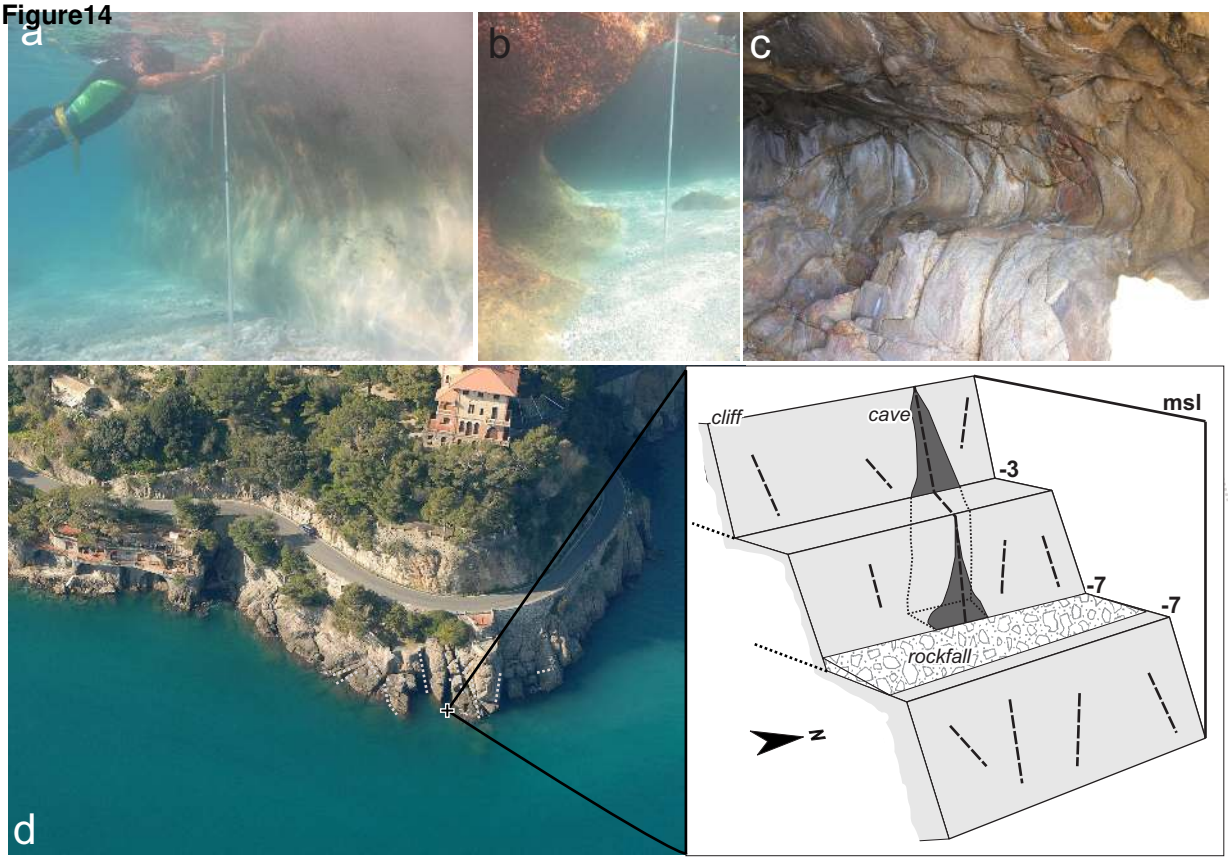

Figure15

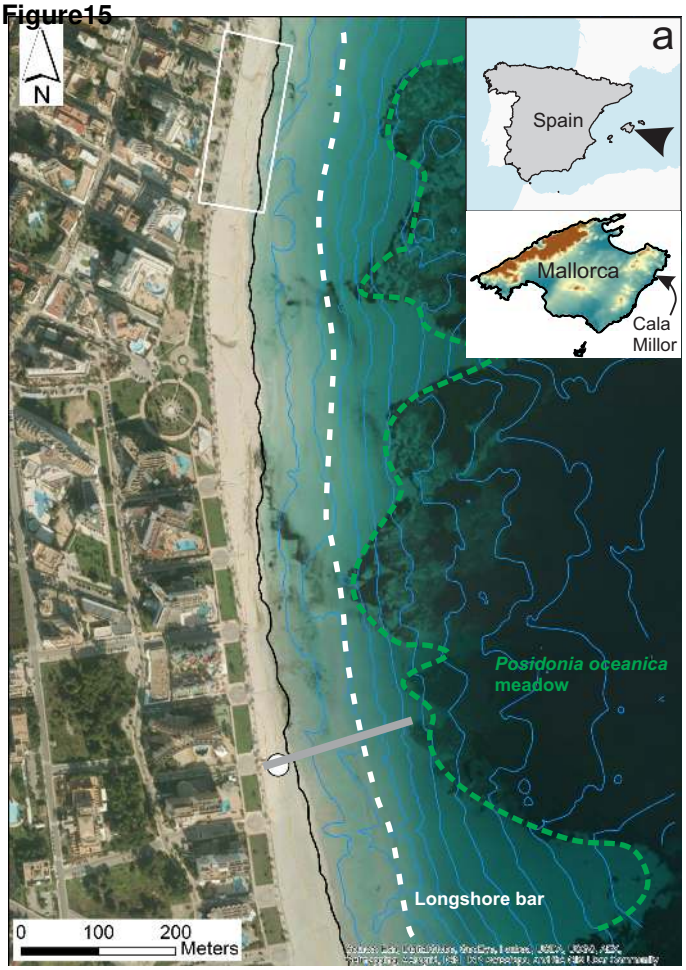
N
a
Spain
Mallorca
Cala
Millor
Posidonia oceanica
meadow
Longshore bar
0
100
200
Meters


1.47±0.02 m
0.97±0.03 m
b

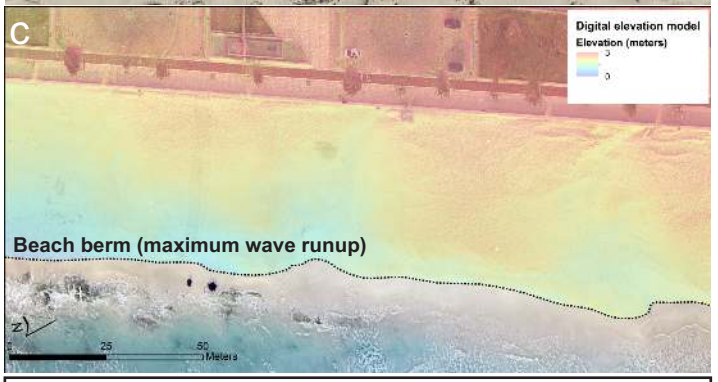
c
Digital elevation model
Elevation (meters)
Beach berm (maximum wave runup)

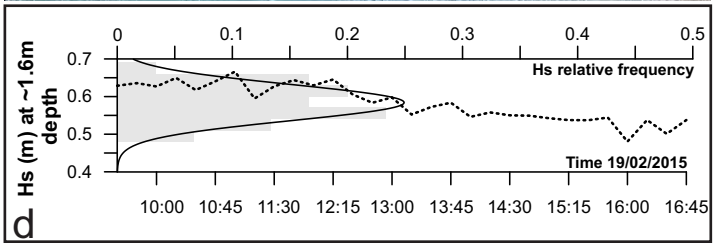
d
Hs (m) at ~1.6m depth
0.7
0.6
0.5
0.4
0
0.1
0.2
0.3
0.4
0.5
Hs relative frequency
Time 19/02/2015
10:00
10:45
11:30
12:15
13:00
13:45
14:30
15:15
16:00
16:45

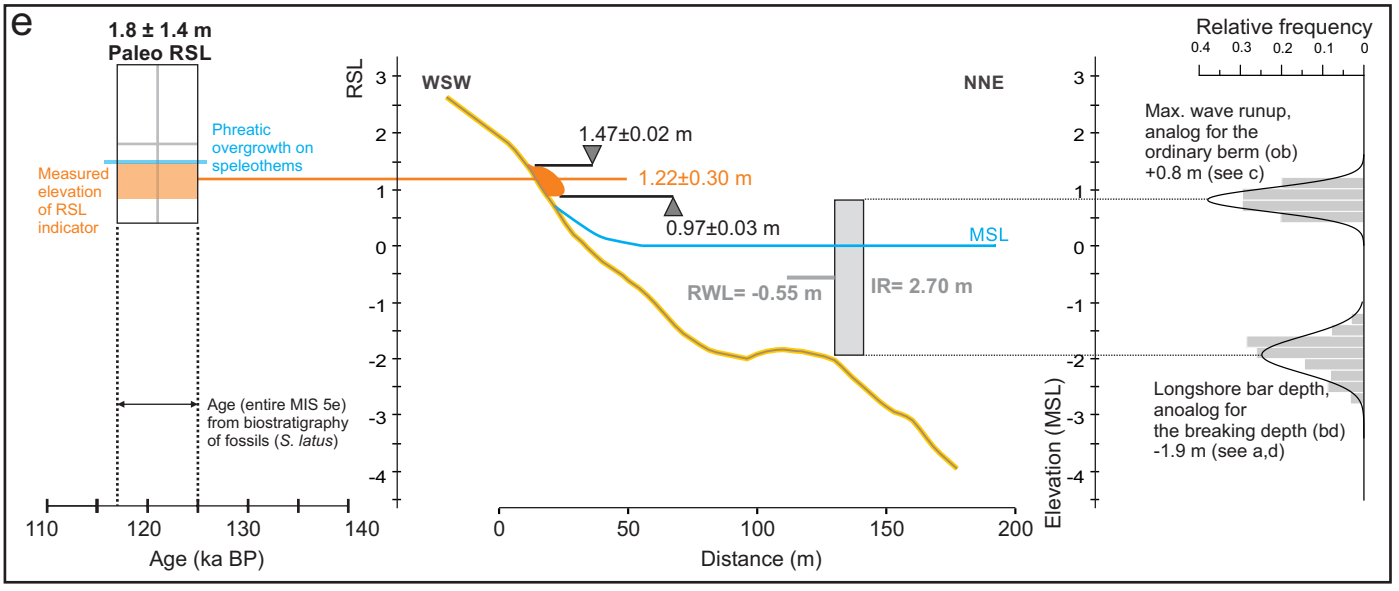
e
1.8 ± 1.4 m
Paleo RSL
Phreatic
overgrowth on
speleothems
Measured
elevation
of RSL
indicator
Age (entire MIS 5e)
from biostratigraphy
of fossils (S. latus)
RSL
Age (ka BP)
110
120
130
140
WSW
NNE
1.47±0.02 m
1.22±0.30 m
0.97±0.03 m
MSL
RWL= -0.55 m
IR= 2.70 m
Distance (m)
0
50
100
150
200
Elevation (MSL)
Relative frequency
0.4
0.3
0.2
0.1
0
Max. wave runup,
analog for the
ordinary berm (ob)
+0.8 m (see c)
Longshore bar depth,
anoalog for
the breaking depth (bd)
-1.9 m (see a,d)

Figure16

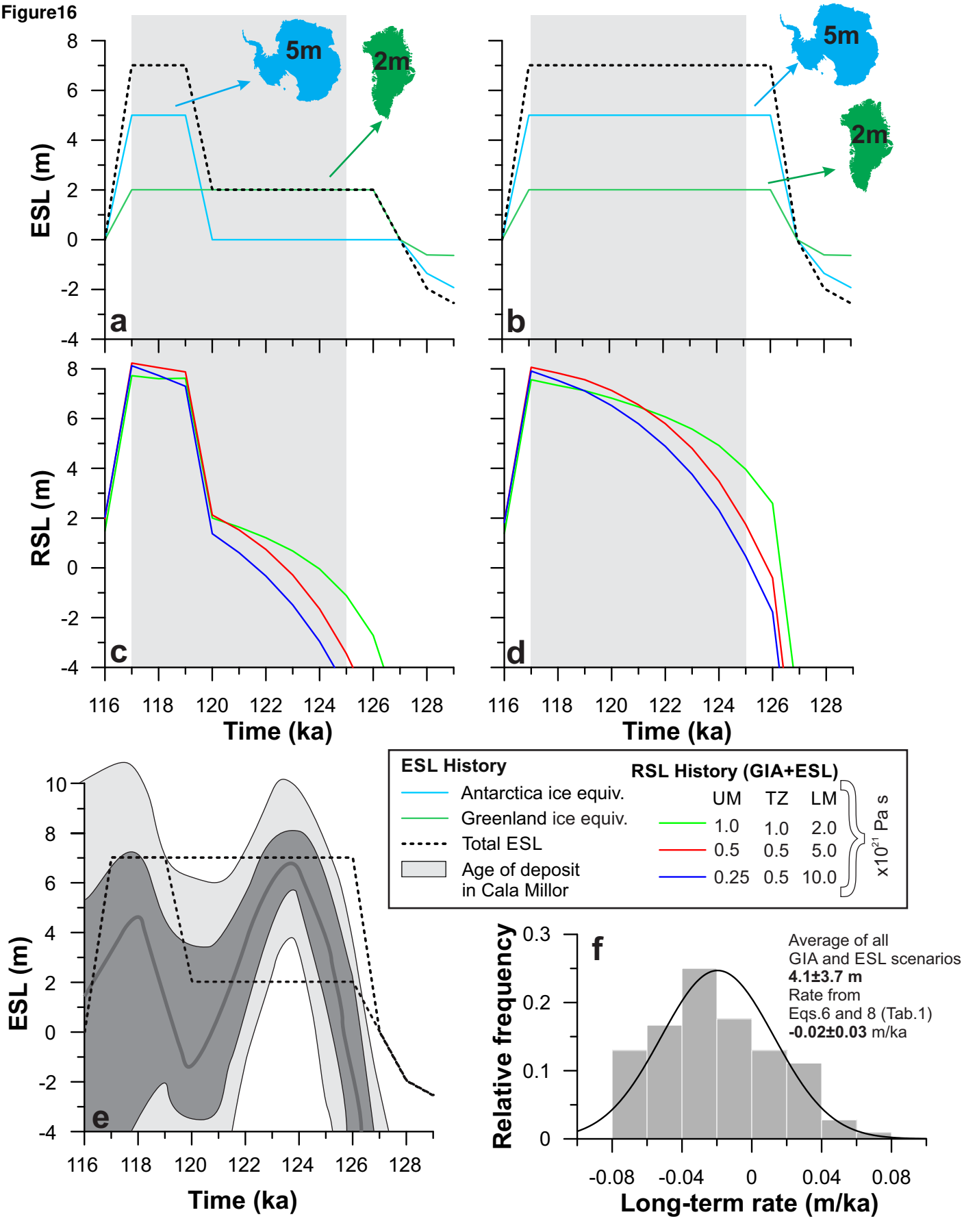
5m
2m
ESL (m)
RSL (m)
a
b
c
d
Time (ka)
ESL History
Antarctica ice equiv.
Greenland ice equiv.
Total ESL
Age of deposit in Cala Millor
RSL History (GIA+ESL)
UM TZ LM
1.0 1.0 2.0
0.5 0.5 5.0
0.25 0.5 10.0
x10^21 Pa s
e
f
Relative frequency
Average of all GIA and ESL scenarios
4.1±3.7 m
Rate from Eqs.6 and 8 (Tab.1)
-0.02±0.03 m/ka
Long-term rate (m/ka)